while *n*-hexane molecules may be adsorbed normal to the surface. We have also found evidence for blocking of the supercage windows due to guest molecule size or orientation.

A complement to this work would be to localize the xenon inside a single supercage either by blocking the channels between the cages or by cooling the sample. Magic angle spinning experiments are under way to compensate for an increase in line width due to the lack of averaging of the anisotropic part of the xenon chemical shift as the temperature is lowered.

Acknowledgment. We thank J. Fraissard and B. F. Chmelka for their comments and suggestions regarding a previous version of this paper. D.R. gratefully acknowledges J. Fraissard for accommodating his stay at the Laboratoire de Chimie des Surfaces in Paris during the spring and summer of 1988, as well as ELF Aquitaine and the Bourse Chateaubriand for financial support. A.P. was a John Simon Guggenheim Fellow. This work was supported by the Director, Office of Energy Research, Office of Basic Energy Sciences, Materials Sciences Division of the U.S. Department of Energy under Contract No. DE-AC03-76SF00098 and by a grant from the Shell Foundation.

Registry No. ^{129}Xe, 13965-99-6; hexane, 110-54-3; benzene, 71-43-2; trimethylbenzene, 25551-13-7.

Consistent Porphyrin Force Field. 1. Normal-Mode Analysis for Nickel Porphine and Nickel Tetraphenylporphine from Resonance Raman and Infrared Spectra and Isotope Shifts

Xiao-Yuan Li,[†] Roman S. Czernuszewicz,[†] James R. Kincaid,[‡] Y. Oliver Su,[†] and Thomas G. Spiro*,[†]

Department of Chemistry, Princeton University, Princeton, New Jersey 08544, and Department of Chemistry, Marquette University, Milwaukee, Wisconsin 53233 (Received: December 20, 1988)

Resonance Raman spectra with variable-wavelength excitation are reported for Ni^{II} porphine (NiP) and for the pyrrole-d_8, meso-d_4, and (pyrrole + meso)-d_{12} isotopomers, as well as for Ni^{II} *meso*-tetraphenylporphine (NiTPP) and its pyrrole-$^{15}N_4$, pyrrole-d_8, $^{13}C_4$-meso, and phenyl-d_{20} isotopomers. All the Raman-active in-plane modes have been identified and are assigned to local coordinates which take into account the phasing of adjacent bond stretches within the pyrrole rings and at the methine bridges. The IR spectra of NiP and its isotopomers are also assigned. For most of the local coordinates good frequency agreement is seen for the different symmetry blocks, showing that longer range phasings have minor effects. These in-plane mode assignments are supported by normal-coordinate calculations with a physically reasonable valence force field, which is nearly the same for NiP and NiTPP. The principal force constants are in good accord with bond length relationships selected on the basis of scaled ab initio calculations. The phenyl substituents of NiTPP lower the frequencies of the asymmetric methine bridge stretching modes $\nu_{10}(B_{1g})$ and $\nu_{19}(A_{2g})$ by $\sim$60 cm^{-1}; this shift is attributable partly to the loss of coupling with the C_mH bending modes in NiP and partly to an electronic effect of the phenyl group. There are also near-resonant interactions in NiTPP between porphyrin and phenyl modes near 740 and 200 cm^{-1} resulting in strongly displaced modes. Otherwise the phenyl groups have little influence on the porphyrin skeletal mode frequencies. Several phenyl modes are subject to moderate RR enhancement, probably via intensity borrowing from nearby porphyrin modes. Large intensities associated with CH bending modes in NiP imply significant excited-state changes in the pyrrole $C_\beta H$ and methine C_mH bond angles. RR spectra for Ni^{II} *meso*-tetramethylporphyrin (TMP) and its methyl-d_{12} isotopomer reveal methyl group modes and somewhat altered skeletal frequencies. Altered polarizations of ν_{10} and ν_{19} in NiTMP and NiTEP (*meso*-tetraethylporphine) reveal a lowering of the effective molecular symmetry, which is attributed to substituent orientation effects. All of these Ni porphyrins show strong overtone and combination band enhancement in resonance with the Q_1 absorption band.

Introduction

Resonance Raman (RR) spectra of metalloporphyrins are of interest[1-13] because of the rich array of spectroscopic phenomena afforded by the electronic properties of the porphyrin chromophore, and also because of the potential for structural characterization in heme proteins. RR spectra of heme proteins have been studied extensively[2] and important regularities have been discovered. It is possible to infer the oxidation, spin, and ligation state of the heme Fe atom with considerable confidence from the frequencies of well-characterized marker bands. No doubt the RR spectra also contain information about more subtle and interesting aspects of heme–protein interactions. Reported spectra of different heme proteins in the same coordination state show numerous differences among bands which have not been well characterized. These differences may be due to protein-imposed distortions of the heme group. It is therefore important to analyze the heme RR vibrational spectrum in as much detail as possible. Ultimately one would like to test structural hypotheses quantitatively with respect to the RR data. Vibrational frequencies for trial structures could be calculated, and compared with experimental data, if a reliable

* Author to whom correspondence should be addressed.
[†] Princeton University.
[‡] Marquette University.

(1) (a) Spiro, T. G.; Li, X.-Y. In *Biological Applications of Raman Spectroscopy*; Spiro, T. G., Ed.; Wiley-Interscience: New York, 1988; Vol. III; Chapter 1. (b) Kitagawa, T.; Ozaki, Y. *Struct. Bonding, Berlin* **1987**, *64*, 71-114.
(2) (a) Spiro, T. G. *Adv. Protein Chem.* **1985**, *37*, 111. (b) Yu, N.-T. *Methods Enzymol.* **1986**, *130*, 350.
(3) (a) Kitagawa, T.; Abe, M.; Ogoshi, H. *J. Chem. Phys.* **1978**, *69*, 4516. (b) Abe, M.; Kitagawa, T.; Kyogoku, Y. *J. Chem. Phys.* **1978**, *69*, 4526.
(4) (a) Choi, S.; Spiro, T. G.; Langry, K. C.; Smith, K. M. *J. Am. Chem. Soc.* **1982**, *104*, 4337. (b) Choi, S.; Spiro, T. G.; Langry, K. C.; Smith, K. M.; Budd, L. D.; La Mar, G. N. *J. Am. Chem. Soc.* **1982**, *103*, 4345. (c) Lee, H.; Kitagawa, T.; Abe, M.; Pandey, R. K.; Leung, H. K.; Smith, K. M. *J. Mol. Struct.* **1986**, *146*, 329.
(5) (a) Willems, D. L.; Bocian, D. F. *J. Am. Chem. Soc.* **1984**, *106*, 880. (b) Willems, D. L.; Bocian, D. F. *J. Phys. Chem.* **1985**, *89*, 234.
(6) Choi, S.; Lee, J. J.; Wei, Y. H.; Spiro, T. G. *J. Am. Chem. Soc.* **1983**, *105*, 3692.
(7) Babcock, G. T. In *Biological Applications of Raman Spectroscopy*; Spiro, T. G., Ed.; Wiley-Interscience: New York, 1988; Vol. III; Chapter 7.
(8) (a) Burke, J. M.; Kincaid, J. R.; Spiro, T. G. *J. Am. Chem. Soc.* **1978**, *100*, 6077 and references therein. (b) Burke, J. M.; Kincaid, J. R.; Peters, S.; Gagne, R. R.; Collman, J. P.; Spiro, T. G. *J. Am. Chem. Soc.* **1978**, *100*, 6083.

0022-3654/90/2094-0031$02.50/0

force field were available, and provided the bands were assigned properly.

We have undertaken a systematic vibrational analysis of nickel porphyrins with different kinds of peripheral substituents, in order to arrive at a consistent mode description and force field for the porphyrin skeleton, and to elucidate the interactions of the skeletal modes with vibrations of the peripheral substituents. Nickel is chosen as the central metal in this comparative study because it forms stable 4-coordinate complexes which are easy to purify and which provide high-quality, fluorescence-free RR spectra. In the present work we analyze the RR and infrared spectra of nickel porphine (NiP), the simplest porphyrin, with H atom peripheral substituents only, and of nickel *meso*-tetraphenylporphyrin (NiTPP), in which phenyl groups replace the H atoms at the methine bridges (see Figure 1 for a structural diagram). Extensive use is made of isotopic frequency shifts involving selective H/D substitution, and, for TPP, ^{15}N in the pyrrole rings and ^{13}C at the methine bridges. TPP is an important member of the porphyrin family because of its ease of synthesis and of crystallization. Much of the information on structure and reactivity in metalloporphyrins derives from metallo TPP studies. There have been numerous reports of metallo TPP RR spectra,[8,9] and a reasonably comprehensive set of assignments has been proposed;[9] calculations have been carried out using porphine force fields, with added phenyl groups.[10] For metalloporphines there have been several measurements and calculations,[11,12] including a quite thorough study of copper porphine.[13] The present study is the first, however, to treat porphine and TPP in a consistent fashion. In addition we examine qualitatively the effect of substituting methyl and ethyl groups at the meso positions instead of phenyl groups.

In the following paper[14a] we reexamine the vibrational spectra of nickel octaethylporphyrin (NiOEP) and extend our force field to it. OEP is important because the substituent pattern is similar to that of physiological porphyrins, and the relationship of metallo-OEP RR spectra to those of heme proteins is easily recognized. Kitagawa and co-workers[3] carried out a pioneering assignment of the NiOEP vibrational spectrum, which has served as a starting point for the elucidation of more complex porphyrins including protoporphyrin,[4] and porphyrins with other unsaturated substituents,[5] as well as heme a.[6,7] A reliable NiOEP force field can serve as a starting point for a rigorous analysis of heme protein spectra.

In the third paper[14b] of this series we present an analysis of the out-of-plane modes of NiOEP, and also NiTPP, while in the fourth paper[14c] the structural dynamics of NiOEP in solution are examined.

Experimental Section

Porphine and Its Deuterated Derivatives. Porphine was purchased from Midcentury Chemical Co. (Posen, IL). The preparation of meso-d_4, pyrrole-d_8, and (meso + pyrrole)-d_{12} deuterated analogues of porphine was accomplished according to the methods described in the literature.[13a] Thus, 20 mg of porphine was converted to porphine-d_{12} by standing in hot (120 °C) 70% $^2H_2SO_4/^2H_2O$ (99% deuterium content) for 90 h. Porphine-d_4 was obtained by treating 10 mg of porphine with concentrated $^2H_2SO_4$ for 18 h at room temperature and porphine-d_8 by similar treatment of 10 mg of porphine-d_{12} sample by H_2SO_4/H_2O. In each case the porphine was isolated from the acid solution and purified as has been previously described.[13a] Nickel was incorporated by the standard procedure in DMF.[15a]

Tetraphenylporphyrin Isotopomers. Tetraphenylporphyrin (TPP) (Aldrich Chemical Co.) was purified by treatment with 2,3-dichloro-5,6-dicyanobenzoquinone (DDQ) followed by column chromatography on alumina (Fisher A-540).[15b,c] TPP-d_8 was synthesized according to the method of Fajer et al.[16a] TPP-d_{20} was synthesized from pyrrole and benzaldehyde-d_5 (98% ^2H Cambridge Isotope Laboratories, Woburn, MA) according to the method of Adler et al.[16b] For TPP-$^{15}N_4$, 0.50 g of pyrrole-^{15}N (95% ^{15}N, Cambridge Isotope Laboratories, Woburn, MA) was reacted with 0.73 mL of benzaldehyde in refluxing propionic acid (28 mL) and isolated according to established procedures.[15a] TPP-$^{13}C_4$ was synthesized by reacting pyrrole (Aldrich) with ^{13}C-labeled benzaldehyde (carbonyl-^{13}C, 99%, Cambridge Isotope Laboratories, Woburn, MA), and similar procedures were followed for TPP-^{15}N. Traces of chlorin were eliminated by treatment with DDQ as described in ref 15b. In each case Ni was incorporated by using the DMF procedure.[15a]

Nickel Tetraalkylporphyrin. TAPs (A = $-CH_3$ for TMP and $-CH_2CH_3$ for TEP) were synthesized and purified according to the method of Ulman et al.[17] TMP-d_{12} was synthesized as follows: 5 g of acetaldehyde-d_4 (99% ^2H, Aldrich) and 4 g of freshly distilled pyrrole were added separately to 300 mL acetic acid at 80–85 °C. The reaction mixture was stirred for 5 h at 80–85 °C and the solvent was evaporated under reduced pressure. The tarry residue was dissolved in ~200 mL of CH_2Cl_2, washed twice with $NaHCO_3$ aqueous solution (5%, dried with Na_2SO_4), and chromatographed with silica gel and neutral aluminum oxide (Grade I), and 200 mg (2% yield) of D_2TMP-d_{12} was obtained. Nickel was incorporated with the DMF procedure.[15a] The final product was checked by NMR showing ~85% deuteration of the $-CH_3$ groups. Chlorin-free NiTPyP was purchased from Midcentury Chemical and used as received.

Spectroscopy. Resonance Raman spectra were obtained with Kr^+ (Spectra Physics, Model 171) and Ar^+ (Spectra Physics 2000-02) ion lasers excited with different lines. Spectra were obtained via backscattering from a spinning (30–50 Hz) NMR tube (solutions) or rotating KCl pellets.[18] The scattered light was collected and analyzed with a Spex 1401 double monochromator equipped with a cooled photomultiplier (RCA 31034A-02) and photon-counting electronics (ORTEC Model 9315). The data were collected digitally with a MINC (DEC) computer. Spectral slit widths were 4 cm^{-1} for spectra below 1700 and 6 cm^{-1} for spectra between 1300 and 3300 cm^{-1}.

UV–vis absorption spectra were obtained with 1-mm quartz cell using a Hewlett-Packard 8450 A diode array spectrophotometer. A DigiLab FTS-20C Fourier transform IR spectrometer was used to collect IR spectra from KBr pellets of solid samples.

Normal-Coordinate Analysis. Normal-mode calculations were performed with the GF matrix method[19a] and a valence force field. Molecualr parameters for NiP and NiTPP were obtained from the crystal structure data of Ni *meso*-tetramethylporphyrin[20] (except that standard H atoms (NiP) or phenyl rings (NiTPP)

(9) Stein, P.; Ulman, A.; Spiro, T. G. *J. Phys. Chem.* **1984**, *88*, 369.
(10) (a) Kozuka, M.; Iwaizomi, M. *Bull. Chem. Soc. Jpn.* **1983**, *56*, 3165. (b) Atamain, M.; Donohoe, R. J.; Lindsey, J. S.; Bocian, D. F. *J. Phys. Chem.* **1989**, *93*, 2236.
(11) (a) Ogoshi, H.; Saito, Y.; Nakamoto, K. *J. Chem. Phys.* **1972**, *57*, 4194. (b) Sunder, S.; Bernstein, H. *J. Raman Spectrosc.* **1976**, *5*, 351.
(12) (a) Susi, H.; Ard, J. S. *Spectrochim. Acta* **1977**, *33A*, 561. (b) Kamisuki, T.; Maeda, S. *J. Raman Spectrosc.* **1976**, *5*, 135.
(13) (a) Gladkov, L. L.; Gradyushko, A. T.; Shulga, A. M.; Solovyov, K. N.; Starukhin, A. S. *J. Mol. Struct.* **1978**, *45*, 267–305; **1978**, *47*, 463. (b) Gladkov, L. L.; Solovyov, K. N. *Spectrochim. Acta* **1985**, *41A*, 1443.
(14) (a) Li, X.-Y.; Czernuszewicz, R. S.; Kincaid, J. R.; Stein, P.; Spiro, T. G. Paper 2 of this series. *J. Phys. Chem.*, following paper in this issue. (b) Li, X.-Y.; Czernuszewicz, R. S.; Kincaid, J. R.; Spiro, T. G. Paper 3 of this series. *J. Am. Chem. Soc.*, in press. (c) Czernuszewicz, R. S.; Li, X.-Y.; Spiro, T. G. Paper 4 of this series. *J. Am. Chem. Soc.*, in press.
(15) (a) Smith, K. M. *Porphyrins and Metalloporphyrins*; Elsevier: New York, 1975. (b) Rousseau, K.; Dolphin, D. *Tetrahedron Lett.* **1974**, *48*, 4251. (c) Barnett, G. H.; Hudson, M. F.; Smith, K. M. *Tetrahedron Lett.* **1973**, *30*, 2887.
(16) (a) Fajer, J.; Borg, D. C.; Forman, A.; Felton, R. H.; Vegh, L.; Dolphin, D. *Ann. N. Y. Acad. Sci.* **1973**, *206*, 349. (b) Adler, A. D.; Longo, F. R.; Finarelli, J. D.; Goldmacher, J.; Assour, J.; Korsakoff, L. *J. Org. Chem.* **1967**, *32*, 476.
(17) (a) Ulman, A.; Gallucci, J.; Fisher, D.; Ibers, J. A. *J. Am. Chem. Soc.* **1981**, *102*, 6852. (b) Ulman, A.; Fisher, D.; Ibers, J. A. *J. Heterocycl. Chem.* **1982**, *19*, 409.
(18) Czernuszewicz, R. S. *Appl. Spectrosc.* **1986**, *40*, 571.
(19) (a) Wilson, E. B.; Decius, J. C.; Gross, P. C. *Molecular Vibrations*; McGraw-Hill: New York, 1955. (b) Schachtschneider, J. H. Shell Development Co., Technical Report No. 51-65 and 231-264, 1962.
(20) (a) Kutzler, F. W.; Swepston, P. N.; Berkovitch-Yellin, Z.; Ellis, D. E.; Ibers, J. A. *J. Am. Chem. Soc.* **1983**, *105*, 2996. (b) Gallucci, J. C.; Swepston, P. N.; Ibers, J. A. *Acta Crystallogr.* **1982**, *838*, 2134.

were substituted for methyl groups), from which Cartesian coordinates were determined via simple trigonometric relationships developed by holding the porphyrin ring planar (D_{4h} symmetry). All atoms of NiTPP phenyl substituents were included in the calculation with phenyl rings oriented perpendicular to the porphyrin plane. The internal coordinate set consisted of Wilson type[19] bond stretching and angle bending for NiP, while that for NiTPP also contained four-atom torsion and out-of-plane wagging coordinates of the phenyl groups. The symmetry coordinates for both porphyrins were taken as symmetry-adapted linear combinations of respective internal coordinates. The porphyrin atom-numbering scheme with corresponding Cartesian coordinates, and the definition of force constants and of internal and symmetry coordinates, are given in the supplementary material.

The potential energy was expressed by a general valence force field which included bond stretching (K), angle bending (H), and valence interaction (f) force constants involving all possible adjacent coordinate pairs sharing at least one atom or pairs which are separated by no more than one atom. The NiTPP force field contained, in addition to K and H constants, out-of-plane wagging (γ), torsion (τ), wagging–wagging ($f(\gamma,\gamma)$), wagging–torsion ($f(\gamma,\tau)$), and torsion–torsion ($f(\tau,\tau)$) interaction force constants of the phenyl substituents. Schachtschneider's programs[19b] were used to construct the G matrices and to solve the secular equations, $|\mathbf{GF} - \mathbf{E}\lambda| = 0$, for each symmetry species on a VAX-11/780 computer. The initial set of principal force constants was transferred from small aromatic rings such as benzene, toluene, pyridine, and pyrrole,[21,22] and stretching constants were scaled with bond distance (see Discussion). Adjacent 1,2 stretch–stretch and stretch–bend interactions were approximated as ~10% of the geometric mean values of the respective principal force constants. Kekule-type, nonadjacent stretch–stretch interactions were initially set all negative and all positive for the 1,3- and 1,4-type interactions, respectively, as established for benzene.[22] The latter constants were found to have negligible effect on the final result and were all set as zero, while the sign of the 1,3 interactions localized within the pyrrole rings was changed (see Discussion). The magnitudes of 1,3 interactions were ~5% of the geometric mean values. The redundancies included in each symmetry species produced zero frequencies in the final result.

The initial set of force constants was first adjusted to reproduce the observed frequencies for NiP and, in particular, its observed isotope shifts (meso-H/D (d_4), pyrrole-H/D (d_8) and (meso + pyrrole)-H/D (d_{12})) by trial and error calculations. Only one or two principal force constants at a time were allowed to vary. These calculations were followed by systematic inclusion of the interaction force constants based on the significance of the particular interaction. Thus, the 1,2 stretch–stretch interactions were added first, which were followed by stretch–bend (sharing two atoms), 1,3 stretch–stretch, stretch–bend (sharing one atom), bend–bend (sharing two atoms) interaction constants, etc. All possible types of valence interactions were tested, and those which produced no or very little effects on the calculated frequencies were excluded from the force field.

Similar trial and error calculations were performed for NiTPP, and for Ni octaethylporphyrin (NiOEP) (see following paper[14a]), using the NiP force field. In fact, all trial calculations involved going back and forth between the three molecules in order to develop a consistent porphyrin force field, capable of reproducing the vibrational spectrum of metalloporphyrins with different substituents. Only small adjustments involving mainly the interaction force constants were needed to fit the NiTPP skeletal vibrational frequencies and to reproduce the pyrrole-H/D (d_8), phenyl-H/D (d_{20}), pyrrole-$^{15/14}N$, and methine-$^{13/12}C$ isotope shifts. The in- and out-of-plane force constants for phenyl substituents were adopted with slight modifications (see Table II) from the published normal-mode analyses on biphenyl.[23] Systematic, partial force constant regressions (each regression involving 8–12 constants) were used to refine the final force field of each molecule.

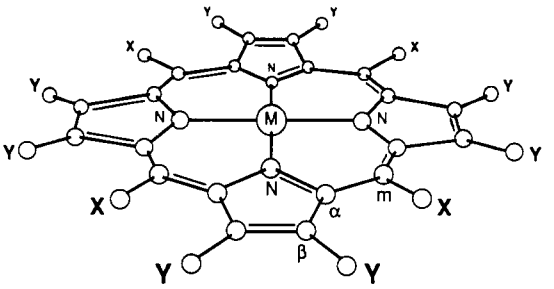

Figure 1. Structural diagram for a D_{4h} metalloporphyrin with generalized peripheral substituents X and Y. The atom labeling scheme ($C_{\alpha,\beta,m}$) is shown.

Results and Discussion

1. Porphyrin Local Coordinates. In assigning the NiOEP vibrational spectra Kitagawa and co-workers[3] adopted a planar D_{4h} molecular model with point mass ethyl substituents. This model can be extended to meso- as well as pyrrole-substituted porphyrins if generalized point mass substituents X (meso) and Y (pyrrole) are assumed at these positions, as illustrated in Figure 1. If the X and Y substituents are actually polyatomic, they will of course have additional vibrational modes. It is convenient to treat these substituent modes separately, making due allowance for the possibility of their mixing with the modes encompassed by the model. The latter include vibrations of the porphyrin skeleton and substituent modes extending as far as the first substituent atom, i.e., C_m–X stretching and bending and C_β–Y stretching and bending. The model has 37 atoms and $2n - 3 = 71$ in-plane degrees of internal freedom which classify as

$$\Gamma_{\text{in-plane}} = 9A_{1g} + 9B_{1g} + 8A_{2g} + 9B_{2g} + 18E_u$$

In analyzing the vibrational modes it is standard practice to use the internal coordinates as a basis, i.e., bond stretchings and angle bendings. We consider it useful, however, to recognize the polycyclic character of the porphyrin ring, and to use "local coordinates" consisting either of individual bond stretching and bending coordinates, with appropriate phasing of symmetry-related pairs, or of collective motions of the 5-membered pyrrole rings. These local coordinates are specified in Figure 2. The pyrrole ring coordinates are a slight variation of the usual ones, which are discussed for example by Colthup et al.,[24] since the outer $C_\beta C_\beta$ bond is essentially a double bond[25] in porphyrins; its stretch is therefore taken as a separate internal coordinate. The stretching motions of the remaining pyrrole bonds are considered collectively, however, and classified according to the phasing. Thus there is a quarter-ring stretch, in which the $C_\alpha C_\beta$ and $C_\alpha N$ bond stretches alternate phase, and two half-ring stretches in which the phases switch at the C_α atoms (producing a mode which is locally symmetric with respect to the pyrrole C_2' axis) or at the N atom (asymmetric). In addition there is a pyrrole breathing mode, in which all of the bonds stretch in phase. The frequencies of these ring stretches are expected to increase with the number of phase alternations, due to kinematic coupling. The number is 0 for the breathing mode, 1 for the asymmetric half-ring stretch, 2 for the symmetric half-ring stretch, and 3 for the quarter-ring stretch.

(21) (a) Pulay, P.; Fogarasi, G.; Boggs, J. E. *J. Chem. Phys.* **1981**, *74*, 3999. (b) Ponder, G.; Fogarasi, G.; Boggs, J. E. *J. Am. Chem. Soc.* **1984**, *106*, 2765. (c) Xie, Y.; Fan, K.; Boggs, J. E. *Mol. Phys.* **1986**, *58*, 401. (d) Niu, Z.; Dunn, K. M.; Boggs, J. E. *Mol. Phys.* **1985**, *55*, 421. (e) Fan, K.; Xie, Y.; Boggs, J. E. *J. Mol. Struct. THEOCHEM.* **1986**, *136*, 339.

(22) (a) Duinker, J. C.; Mills, I. M. *Spectrochim. Acta* **1968**, *24A*, 417. (b) LaLau, C.; Snyder, R. G. *Spectrochim. Acta* **1968**, *27A*, 2073. (c) Scott, D. N. *J. Mol. Spectrosc.* **1969**, *31*, 451; **1971**, *37*, 77. (d) Berezin, V. I. *Opt. Spectrosc. (Engl. Transl.)* **1963**, *15*, 167. (e) Cummings, D. L.; Wood, J. L. *J. Mol. Struct.* **1979**, *20*, 1. (f) Neto, N.; Scrocco, M.; Califano, S. *Spectrochim. Acta* **1966**, *22*, 1981. (g) Ohno, K. *J. Mol. Spectrosc.* **1978**, *72*, 238.

(23) (a) Zerbi, G.; Sandroni, S. *Spectrochim. Acta* **1968**, *24A*, 483, 511. (b) Eaton, V. J.; Steele, D. *J. Chem. Soc., Faraday Trans. 2* **1973**, *69*, 1601. (c) Eaton, S. S.; Eaton, G. R. *J. Am. Chem. Soc.* **1975**, *97*, 3660.

(24) Colthup, N. B.; Daley, L. H.; Wiberley, S. E. *Introduction to Infrared and Raman Spectroscopy*; Academic Press: New York, 1975; p 274.

(25) Hoard, J. L. In *Porphyrins and Metalloporphyrins*; Smith, K. M., Ed.; Elsevier: New York, 1975; pp 317–376.

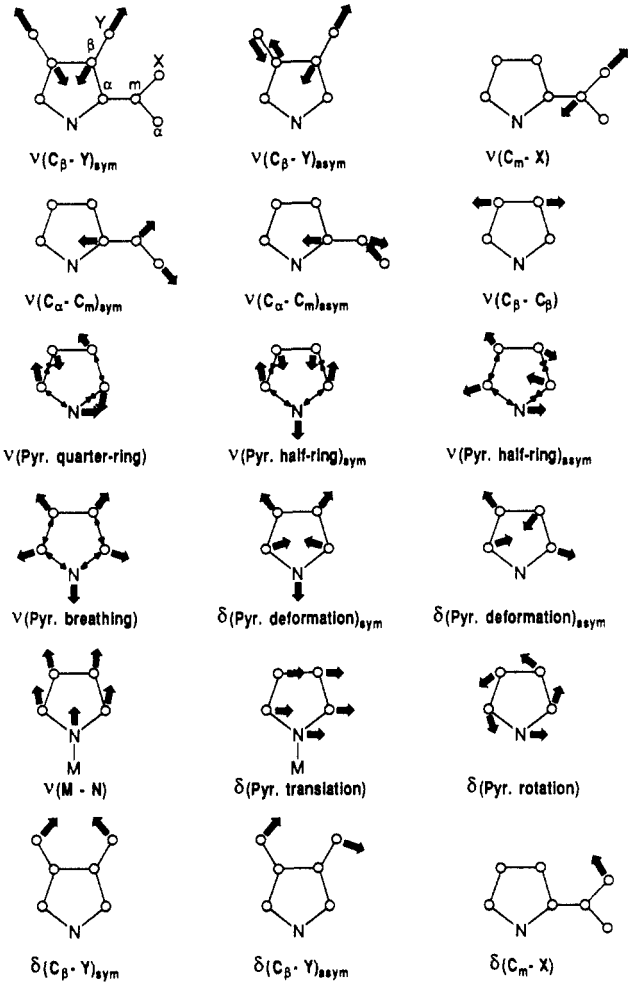

Figure 2. Illustration of the local coordinates used in classifying the in-plane porphyrin skeletal modes. The stretching motions of the $C_\alpha N$ and $C_\alpha C_\beta$ pyrrole bonds are considered collectively (see text), and classified according to the phases of the individual bonds shown by light arrows.

In addition there are two pyrrole in-plane deformation modes, which are symmetric and asymmetric with respect to the C_2' axis. When these pyrrole internal coordinates are added to internal coordinates for C_m–X stretching and bending, C_β–Y stretching and bending, and C_α–C_m and N–Ni stretching, the coordinate set can be completed by adding rotation and translation coordinates for the pyrrole rings taken as rigid units (see Figure 2); the radial translation of the pyrrole rings is redundant with the N–M stretch.

Table I shows a classification of these coordinates into the symmetry species. The entries are the actual mode numbers used in the subsequent analysis. Standard usage is to number the individual modes within each symmetry block in order of descending frequency. Kitagawa and co-workers[3] applied this numbering scheme to NiOEP, and it has been widely adopted for band notation in vibrational studies of physiological type porphyrins, i.e., those with carbon substituents at the pyrrole positions. We seek to extend the correspondence of the NiOEP mode numbers to analogous skeletal modes of NiP and NiTPP. This requires deviation from a strict frequency order since the highest frequency modes, which involve C–H stretching, are found in different symmetry blocks depending on whether X or Y = H. Likewise the C_m–X and C_β–Y bending frequencies are much higher when X, Y = H than when heavier substituents are involved.

2. Force Fields. Valence force fields were used to calculate the vibrational frequencies and isotope shifts for NiP and NiTPP. Valence force constants are more transferable between similar structures than are Urey–Bradley force constants, especially for aromatic molecules where interactions between nonadjacent internal coordinates have to be included.[26a] The observed frequencies and isotope shifts (discussed below) were all fit to reasonable accuracy with the force constants listed in Table II. Details of the calculation, including the definition of force constants and of internal and symmetry coordinates, are given in the supplementary material. Particular attention was paid to reproducing the isotope shift pattern, in order to obtain realistic mode compositions. We view this as a more important objective than exact agreement between observed and calculated frequencies. To arrive at this force field we initially transferred force constants from previous analyses of aromatic molecules, including benzene, toluene, pyrrole, and pyridine.[21,22] The principal bond stretching force constants were scaled with bond distance. Several empirical force constant/bond length relationships have been proposed.[26b-h] These have similar shapes but give appreciably different values of the force constant for a given distance. To gauge the reliability of these relations, we examined the recently available scaled ab initio force constants which give accurate results for small molecules.[26i-k] We find that for CC bonds the ab initio force constants are well described by the empirical curves of Johnston,[26g] and of Burgi and Dunitz,[26h] as well as of Susi and Ard,[26d] which are nearly superimposable, while the CN ab initio force constants fall between the curves given by Badger[26b] and Herschbach and Laurie,[26c] and by Byler et al.;[26e] these curves are shown in Figure 3. Our final principal force constants are shown in Figure 3 to be in satisfactory agreement with these relationships, analytical functions for which are given in the Figure 3 caption.

The effects of different types of interaction constants were

TABLE I: Local Coordinate Contributions to the Normal Modes in a D_{4h} Metalloporphyrin[a]

local coordinate[b]	A_{1g}	B_{1g}	A_{2g}	B_{2g}	E_u
$\nu(C_mX)$	ν_1			ν_{27}	ν_{36}
$\nu(C_\alpha C_m)_{asym}$[c]		ν_{10}	ν_{19}		ν_{37}
$\nu(C_\beta C_\beta)$	ν_2	ν_{11}			ν_{38}
$\nu(C_\alpha C_m)_{sym}$	ν_3			ν_{28}	ν_{39}
ν(Pyr quarter-ring)			ν_{20}	ν_{29}	ν_{40}
ν(Pyr half-ring)$_{sym}$	ν_4	ν_{12}			ν_{41}
$\delta(C_mX)$		ν_{13}	ν_{21}		ν_{42}
$\nu(C_\beta X)_{sym}$	ν_5	ν_{14}			ν_{43}
ν(Pyr half-ring)$_{asym}$			ν_{22}	ν_{30}	ν_{44}
$\nu(C_\beta Y)_{asym}$			ν_{23}	ν_{31}	ν_{45}
δ(Pyr def)$_{asym}$			ν_{24}	ν_{32}	ν_{46}
ν(Pyr breathing)	ν_6	ν_{15}			ν_{47}
δ(Pyr def)$_{sym}$	ν_7	ν_{16}			ν_{48}
δ(Pyr rot)			ν_{25}	ν_{33}	ν_{49}
ν(NM)[d]	ν_8	ν_{18}			ν_{50}
$\delta(C_\beta Y)_{asym}$			ν_{26}	ν_{34}	ν_{51}
$\delta(C_\beta Y)_{sym}$	ν_9	ν_{17}			ν_{52}
δ(Pyr transl)[e]			f	ν_{35}	ν_{53}
total modes:	9	9	8	9	18

[a] The classification is based on a 37-atom metalloporphyrin core consisting of 25 skeletal atoms and of only first atoms of the 12 peripheral substituents (8 at C_β(Y) and 4 at C_m(X) positions, see Figure 1). The substituent internal moddes are considered separately (see text). [b] See Figure 2 for the definition of the local coordinates. [c] Subscripts sym and asym refer to combinations of the indicated coordinate that are symmetric or asymmetric with respect to the C_2' (passing through the N atoms) or C_2'' (passing through the C_m atoms) axes. [d] Translations of the pyrrole (Pyr) rings radially are redundant with the M–N stretch. [e] Translations of the pyrrole rings tangentially. [f] Redundant with the whole molecule rotation.

(26) (a) Califano, S. *Vibrational States*; Wiley: New York, 1976; Chapter 8. (b) Badger, R. M. *J. Chem. Phys.* **1935**, *3*, 710. (c) Herschbach, D. R.; Laurie, V. W. *J. Chem. Phys.* **1961**, *35*, 458. (d) Susi, H.; Ard, J. S. *Spectrochim. Acta* **1971**, *27A*, 1549. (e) Byler, D. M.; Susi, H.; Damert, W. C. *Spectrochim. Acta* **1987**, *43A*, 861. (f) Conradson, S. D.; Sattelberger, A. P.; Woodruff, W. M. *J. Am. Chem. Soc.* **1988**, *110*, 1309. (g) Johnston, H. S. *J. Am. Chem. Soc.* **1964**, *86*, 1643. (h) Burgi, H.-B.; Dunitz, J. D. *J. Am. Chem. Soc.* **1987**, *109*, 2924. (i) Fogarasi, G.; Pulay, P. *Annu. Rev. Phys. Chem.* **1984**, *35*, 191. (j) Hess, B. A., Jr.; Schaad, L. J.; Carsky, P.; Zahradnik, R. *Chem. Rev.* **1986**, *86*, 709. (k) Tsuboi, M.; Nishimura, Y.; Hirakawa, A. Y.; Peticolas, W. In *Biological Applications of Raman Spectroscopy*; Spiro, T. G., Ed.; Wiley-Interscience: New York, 1987; Vol. 2, Chapter 3. (l) Sellers, H.; Pulay, P.; Boggs, J. E. *J. Am. Chem. Soc.* **1985**, *107*, 6487.

TABLE II: Valence Force Constants for NiP and NiTPP[a]

$K(R_i)$/(mdyn/Å)	$H(\alpha_j)$/(mdyn Å/rad^2)	interaction force constants[b]
		Porphyrin Core
$K(C_\beta C_\beta)_1 = 7.12$	$H(C_\alpha NC_\alpha)_1 = 1.53$	$f_{1,2}(R_i,R_i)$: $f(1,4) = 0.45$ (0.70); $f(2,2) = 0.30$ (0.60); $f(2,3) = 0.30$ (0.60); $f(2,4) = 0.40$ (0.60); $f(2,5) = 0.00$ (0.30); $f(3,3) = 0.45$ (0.60); $f(3,4) = 0.45$ (0.50); $f(3,7) = 0.30$ (0.40); $f(7,7) = 0.15$
$K(C_\alpha C_m)_2 = 6.98$	$H(C_\beta C_\beta C_\alpha)_2 = 1.37$	$f(7,7) = 0.15$
$K(C_\alpha N)_3 = 5.64$	$H(C_\beta C_\alpha N)_3 = 1.50$	$f_{1,3}(R_i,R_i)$: $f(1,2) = -0.35$ (−0.30); $f(2,3) = f(2,4) = -0.10$(−0.15); $f(2,7) = -0.20$(−0.15)
$K(C_\alpha C_\beta)_4 = 5.27$ (5.02)	$H(C_\alpha C_m C_\alpha)_4 = 1.45$ (1.25)	$f_{1,3}'(R_i,R_i)$: $f(1,3) = f(3,4) = f(4,4) = 0.20$
$K(C_mX)_5 = 5.02$ (4.90)	$H(C_\beta C_\alpha C_m)_5 = 0.83$	$f_1(R_i,\alpha_j)$: $f(2,3) = f(3,5) = f(4,6) = -0.22$ (−0.25); $f(2,9) = 0.00$ (−0.10); $f(3,9) = 0.07$; $f(4,7) = -0.10$ (−0.05)
$K(C_\beta H)_6 = 5.20$	$H(NC_\alpha C_m)_6 = 0.83$	$f(2,8) = f(3,8) = f(4,7) = f(4,9) = -0.03$; $f(3,2) = f(3,3) = f(3,4) = f(3,6) = f(4,1) = -0.10$ (−0.12)
$K(NiN)_7 = 1.68$	$H(C_\beta C_\beta H)_7 = 0.454$	$f_2(R_i,\alpha_j)$: $f(1,2) = 0.25$ (0.30); $f(2,4) = 0.25$ (0.20); $f(2,5) = 0.30$ (0.20); $f(2,9) = 0.05$ (0.10); $f(3,1) = f(4,2) = f(4,3) = f(4,5) = 0.25$; $f(3,3) = 0.10$ (0.30); $f(3,6) = f(2,10) = f(1,7) = 0.10$
	$H(C_\alpha C_\beta H)_8 = 0.454$	$f(4,9) = 0.10$ (0.15)
	$H(C_\alpha C_m X)_9 = 0.462$ (1.00)	$f_1(\alpha_j,\alpha_j)$: $f(2,4) = f(5,5) = f(6,6) = 0.15$
	$H(C_\alpha NNi)_{10} = 0.30$	$f_2(\alpha_j,\alpha_j)$: $f(2,3) = -0.10$; $f(3,6) = f(5,6) = 0.10$ (0.05); $f(4,9) = 0.10$ (0.20); $f(7,8) = 0.01$ (0.00)
	$H(NNiN)_{11} = 0.25$	
		Phenyl Substituents
in-plane[c]		
$K(CC)_8 = 6.312$	$H(CCC)_{12} = 0.959$	$f_{1,2}(R_i,R_i)$: $f(5,8) = 0.150$; $f(8,8) = 0.740$
$K(CH)_9 = 5.116$	$H(CCC_m)_{13} = 0.755$	$f_{1,3}(R_i,R_i)$: $f(8,8) = -0.346$
	$H(CCH)_{14} = 0.535$	$f_{1,4}(R_i,R_i)$: $f(8,8) = 0.30$
		$f_1(R_i,\alpha_j)$: $f(5,13) = 0.250$
		$f_2(R_i,\alpha_j)$: $f(8,13) = 0.108$; $f(8,14) = 0.25$
out-of-plane[d]		
	$\gamma(CH)_{15} = 0.270$	$f(\gamma_i,\gamma_j)$: $f_o(15,15) = 0.025$; $f_m(15,15) = -0.005$; $f_p(15,15) = 0.035$
	$\tau(CC)_{16} = 0.160$	$f(\gamma_j,\tau_j)$: $f_o(15,16) = -0.02$; $f_m(15,16) = -0.005$
	$\tau(C_1C)_{17} = 0.250$	$f_2(\tau_j,\alpha_j)$: $f(18,4) = f(18,12) = -0.30$
	$\tau(C_mC_1)_{18} = 0.05$[e]	$f(\tau_j,\tau_j)$: $f_o(16,16) = -0.005$

[a] $K(R_i)$ and $H(\alpha_j)$ are principal stretching and bending force constants for the indicated bonds and angles. The subscripted numbers are used to label the interaction force constants. Most force constants are common for NiP and NiTPP; where different values were used, the NiTPP force constant is given in parentheses next to the corresponding NiP value. [b] Stretch–stretch interactions in mdyn/Å; stretch–bend interactions in mdyn/rad; bend–bend interactions in mdyn Å/rad^2. $f_{1,2}(R_i,R_l)$ = 1,2 stretch–stretch interactions (common α_j); e.g. $f(1,4) = f_{1,2}(C_\beta C_\beta, C_\alpha C_\beta)$. $f_{1,3}(R_i,R_i)$ = 1,3 stretch–stretch interactions between pyrrole ring and the methine bridge; e.g., $f(1,2) = f_{1,3}(C_\beta C_\beta, C_\alpha C_m)$. $f_{1,3}(R_i,R_i)$ = 1,3 stretch–stretch interactions within the pyrrole ring; e.g., $f(1,3) = f_{1,3}(C_\beta C_\beta, C_\alpha N)$. $f_1(R_i,\alpha_j)$ = stretch–bend interactions between R_i and α_j sharing one common atom; e.g., $f(2,3) = f_1(C_\alpha C_m, C_\beta C_\alpha N)$. $f_2(R_i,\alpha_j)$ = stretch–bend interactions between R_i and α_j sharing two common atoms; e.g. $f(1,2) = f_2(C_\beta C_\beta, C_\beta C_\beta C_\alpha)$. $f_1(\alpha_j,\alpha_i)$ = bend–bend interactions between α_j's sharing one common atom; e.g., $f(2,4) = f_1(C_\beta C_\beta C_a, C_\alpha C_m C_\alpha)$. $f_2(\alpha_j,\alpha_j)$ = bend–bend interactions between α_j's sharing two common atoms; e.g., $f(2,3) = f_2(C_\beta C_\beta C_\alpha, C_\beta C_\alpha N)$. [c] Simplified in-plane valence force field for phenyl vibrations was transfered from the work on biphenyl by Zerbi and Sandroni (ref 23a): the phenyl–phenyl inter-ring interaction force conntants were modified slightly to describe the porphyrin–phenyl interactions. [d] The out-of-plane phenyl force field was transfered from the work on biphenyl by Eaton and Steele (ref 23b) with slight modifications of the inter-ring interaction force constants. $\gamma(CH)$ = out of the phenyl plane C–H bond wagging. The six-atom torsional force constants (ϕ type) from ref 23b were transformed to four-atom torsional force constants (τ type) and used in this calculation, with slight modifications. $\tau(CC)$ = C–C–C–C torsions within the phenyl rings; $\tau(C_1C)$ = C_m–C_1–C–C torsions which are equivalent to $\gamma(C_1C_m)$ out-of-plane wagging of C_1–C_m bond relative to porphyrin ring; $\tau(C_mC_1)$ = C_α–C_m–C_1–C and C_β–C_m–C_1–C torsions. $f(\gamma_j,\gamma_j)$ = out-of-plane wag-wag interactions between γ_j's within the phenyl rings; f_o,f_m, and f_p refer to interactions of the two indicated coordinates at respectively ortho, meta, and para positions on a given phenyl ring. $f(\gamma_j,\tau_j)$ = out-of-plane wag–torsion interactions between γ_j and τ_j within the phenyl rings. $f_2(\tau_j,\alpha_j)$ = torsion–bend interactions between τ_j and α_j sharing two common atoms. $f(\tau_j,\tau_j)$ = torsion–torsion interactions within the phenyl rings. [e] This force constant describes the phenyl ring rotation around the C_m–C_{Ph} bond. Its value, 0.05 mdyn A/rad^2, is estimated from a one phenyl rotational barrier of about 15 kcal/mol reported in literature (ref 23c and references therein).

examined systematically in trial calculations. As far as possible, all interaction constants of a given type were held at the same value. In aromatic systems such as benzene, stretch–stretch interaction constants are expected to be positive for adjacent bonds (1,2 interactions); the ab initio calculations give values which are 7–12% of the geometric mean of the principal force constants. All of the porphyrin 1,2 interaction constants are positive (Table II), and their magnitudes are less than 10% of the principal constant mean. The 1,3 interaction constants are less than 5% of the 1,3 geometric mean. They are negative throughout the 16-membered inner and 18-membered outer aromatic (Figure 1) ring but are positive within the pyrrole rings, perhaps reflecting the competition between the two delocalization pathways. In support of this inference we note that negative as well as positive 1,3 interaction constants have been obtained by ab initio calculations on polycyclic molecules, naphthalene[26l] and purines.[26k]

We tried to keep the skeletal force field as constant as possible between porphine and TPP since the substituents have little influence on the ring structure, according to Hoard.[25] Some electronic differences are expected, however, upon replacing H atoms with phenyl groups. We allowed force field changes to be accommodated by relatively small alterations of the interaction constants, keeping the same set of diagonal force constants for NiP and NiTPP, except for the $C_\alpha C_\beta$ bond stretching constant, which had to be lowered slightly to fit the pyrrole ring mode frequencies.

A direct comparison of the NiP and NiTPP structure parameters is not possible. No crystal structure has been reported for NiP, while the structure of NiTPP has been determined only to the level of establishing isomorphism with CuTPP.[27] Crystal structures of the free bases of these porphyrins have been determined[28] and show slight bond distance differences, but the

(27) Fleischer, E. B.; Miller, C. K.; Webb, L. E. *J. Am. Chem. Soc.* **1964**, *86*, 2342.

(28) (a) Silvers, S. J.; Tulinsky, A. *J. Am. Chem. Soc.* **1967**, *89*, 3331. (b) Chen, B. M. L.; Tulinsky, A. *J. Am. Chem. Soc.* **1972**, *94*, 4144. (c) Lauher, J. W.; Ibers, J. A. *J. Am. Chem. Soc.* **1973**, *95*, 5148.

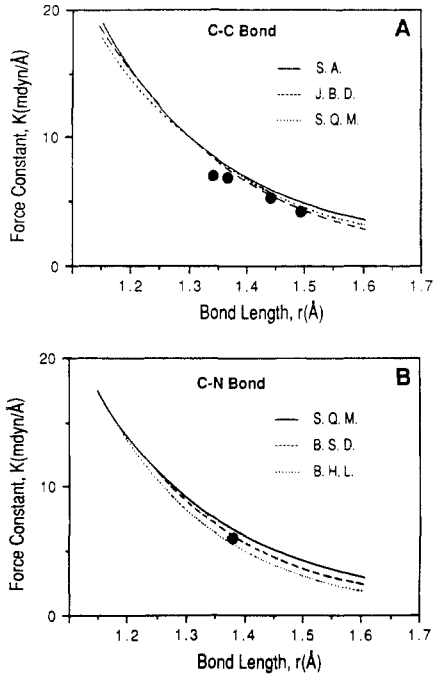

Figure 3. Force constant/bond length relationships for (A) CC bonds and (B) CN bonds. The force constant values used in the present calculation are shown by filled cycles. The curves are drawn according to the $K = \alpha \times 10^{-\beta r}$ relationship with the following α and β values. CC bonds: JBD (Johnston,[26g] Burgi and Dunitz[26h]) $\alpha = 2300.5$, $\beta = 1.8169$; SA (Susi and Ard[26d]) $\alpha = 1487.3$, $\beta = 1.6563$; SQM (scaled quantum mechanical force constants[26i-k]) $\alpha = 1606.9$, $\beta = 1.6976$. CN bonds: BHL (Badger,[26b] and Herschbach and Laurie[26c]) $\alpha = 2629.4$, $\beta = 1.9255$; BSD (Byler, Susi, and Damert[26e]) $\alpha = 1520.9$, $\beta = 1.7000$; SQM (scaled quantum mechanical force constants[26i-k]) $\alpha = 2929.0$, $\beta = 1.9366$.

TABLE III: Structural Parameters Used in Normal-Coordinate Analysis of NiP and NiTPP[a]

bond	length, Å	bond	angle, deg
	Porphyrin Core		
C_β–C_β	1.352	N–Ni–N	90.0
C_α–C_m	1.383	C_α–N–Ni	127.6
C_α–C_β	1.440	N–C_α–C_β	110.7
C_α–N	1.380	C_α–C_β–C_β	106.8
N–Ni	1.955	C_α–N–C_α	104.8
C_m–H	1.090	N–C_α–C_m	126.5
C_m–C_{Ph}	1.509	C_β–C_α–C_m	122.8
		C_α–C_m–C_α	121.4
		C_α–C_m–C_{Ph}	119.3
		C_α–C_β–H	128.0[b]
		C_β–C_β–H	125.2[b]
	Phenyl Substituents		
C–C	1.380	C–C–C	120.0
C–H	1.090	C_m–C–C	120.0
		C–C–H	120.0

[a] Taken from the crystal structure of Ni *meso*-tetramethylporphyrin[20] with slight adjustments to maintain a D_{4h} symmetry of the porphyrin core. [b] Estimated values from X-ray structure of Ni octaethylporphyrin.[45]

degree of ruffling is also markedly different. Consequently we adopted the structural parameters of nickel *meso*-tetramethylporphyrin,[20] listed in Table III, for both calculations (except, of course, that standard H atoms or phenyl rings were substituted for the methyl groups).

Least-squares fitting of the frequencies was carried out only after a good preliminary fit to the data was obtained in the trial calculations. Eight to twelve force constants at a time were allowed to vary, since global regressions always diverged. The final porphine force field contained 35 free-adjustable force constants (18 principal and 17 interaction), and reproduced the 154 observed frequencies (including isotopic frequencies) with an average error of 12 cm^{-1}. The TPP force field contained 36 free-adjustable

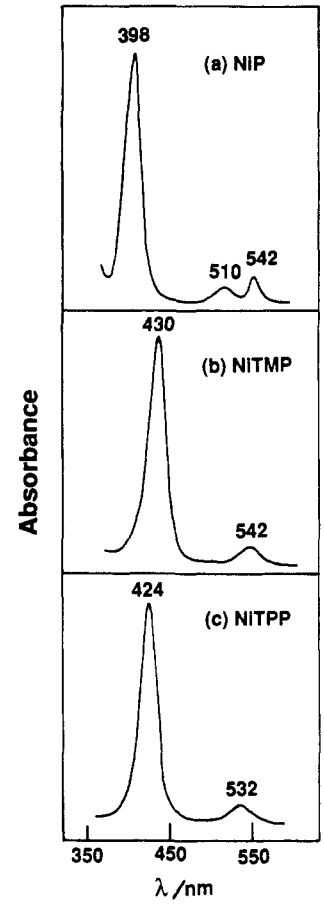

Figure 4. Absorption spectra of the indicated nickel porphyrin in CS_2 solution.

constants for the porphyrin core (18 principal and 18 interaction), and an additional 24 force constants for the phenyl rings, and reproduced the 174 observed frequencies with an average error of 11 cm^{-1}.

Our NiP force field differs significantly from the Cu porphine force field reported by Gladkov and Solovyov,[13] even though the quality of the frequency fitting is similar in the two studies. These differences reflect the well-known fact that force fields are not unique with respect to the fitting of frequencies in polyatomic molecules of even moderate complexity.[26a] We found it impossible, however, to calculate the observed TPP frequencies and isotope shifts with the force field of Gladkov and Solovyov,[13] without major alterations. Thus we feel that our force field gives a better representation of the vibrational mode structure of the porphyrin skeleton. We note also that the interaction constants employed by Gladkov and Solovyov have a wide range of values, some of which seem unreasonably large.

3. Resonance Raman Enhancement Pattern. Figure 4 shows the absorption spectrum of NiP, as well as NiTPP and NiTMP, in CS_2. The usual three-banded spectrum is seen for NiP with the B (Soret), Q_1 (β), and Q_0 (α) bands at 398, 510, and 542 nm. For the meso substituted Ni porphyrins, the B band is observed at ~425 nm while the Q band region is dominated by Q_1 at ~535 nm; Q_0 is much weaker and appears as a shoulder at ~565 nm. Excitation wavelengths at 406.7, 413.1, 514.5, 530.9, and 568.2 nm, in resonance with the B and Q bands, were used to produce the RR spectra of NiP and NiTPP shown in Figures 5–13.

The very different enhancement patterns for these excitation wavelengths can be understood[1] in relation to the first two π–π^* porphyrin excited states, which are well described by Gouterman's four-orbital model.[29] The two highest filled orbitals, a_{2u} and a_{1u}, are nearly degenerate, and the excitations to the degenerate pair

(29) Gouterman, M. In *Porphyrins*; Dolphin, D., Ed.; Academic Press: New York, 1979; Vol. III, Part A, pp 1–156.

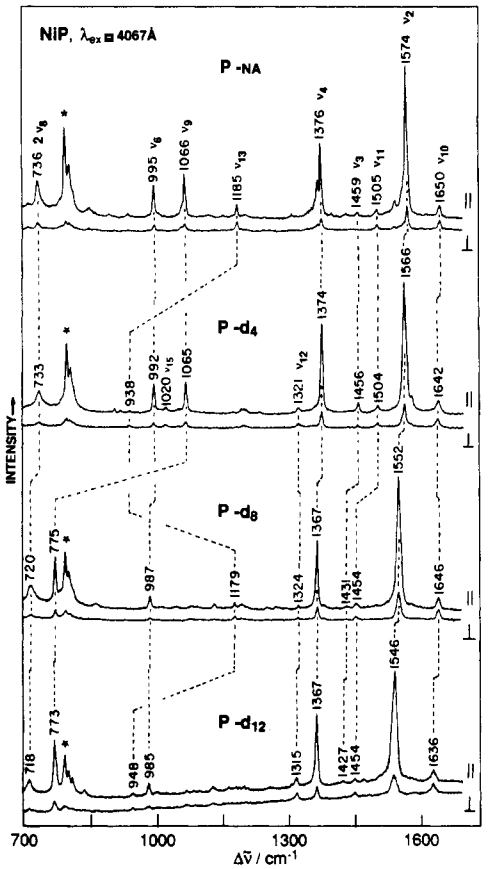

Figure 5. RR spectra with 4067-Å excitation in the 700–1700-cm^{-1} region for Ni porphine (NA = natural abundance) and its meso-d_4, pyrrole-d_8, and (meso + pyrrole)-d_{12} isotopomers in CS_2 solution, in parallel (∥) and perpendicular (⊥) polarization. Conditions: 150 mW laser power; 4 cm^{-1} slit width; 1 scan with increment of 0.5 cm^{-1}/s. The A_{1g} (p) and B_{1g} (dp) modes are labeled. * = solvent band.

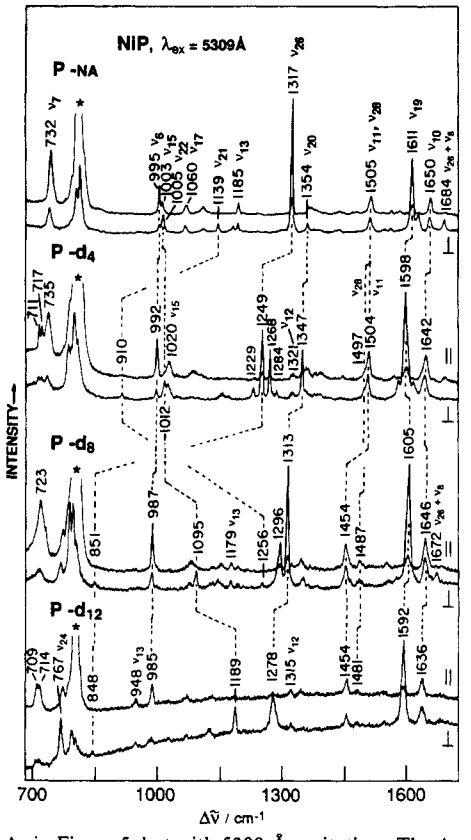

Figure 6. As in Figure 5, but with 5309-Å excitation. The A_{2g} (ap), B_{1g} and B_{2g} (dp) modes are labeled.

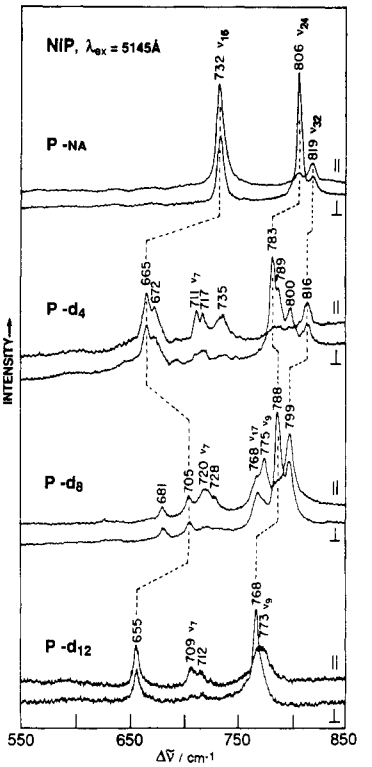

Figure 7. As in Figure 5, but 550–850-cm^{-1} region with 5145-Å excitation. A THF solution instead of CS_2 was used because of interference from strong CS_2 bands at 660 and 800 cm^{-1}.

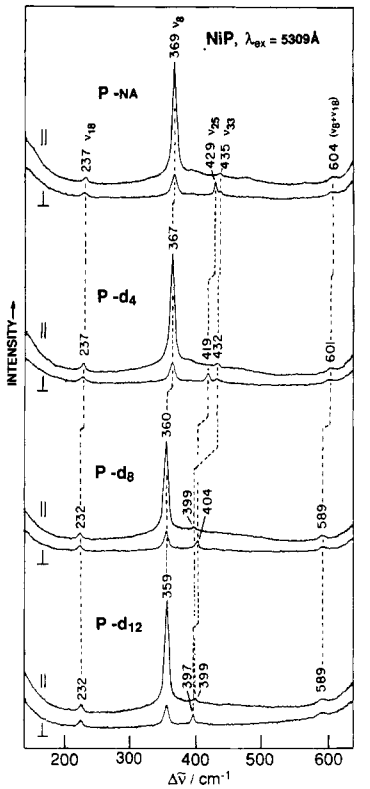

Figure 8. As in Figure 5, but 200–600-cm^{-1} region with 5309-Å excitation.

of lowest empty orbitals, e_g^*, undergo strong configurational interaction, producing well-separated states, at ~400 and ~550 nm. The transition dipoles add for the higher energy transition to produce the very strong B absorption band and nearly cancel for the lower energy transition producing the much weaker Q_0 band. These transitions also mix vibronically, producing the Q_1 absorption sideband, which peaks ~1300 cm^{-1} above Q_0 and

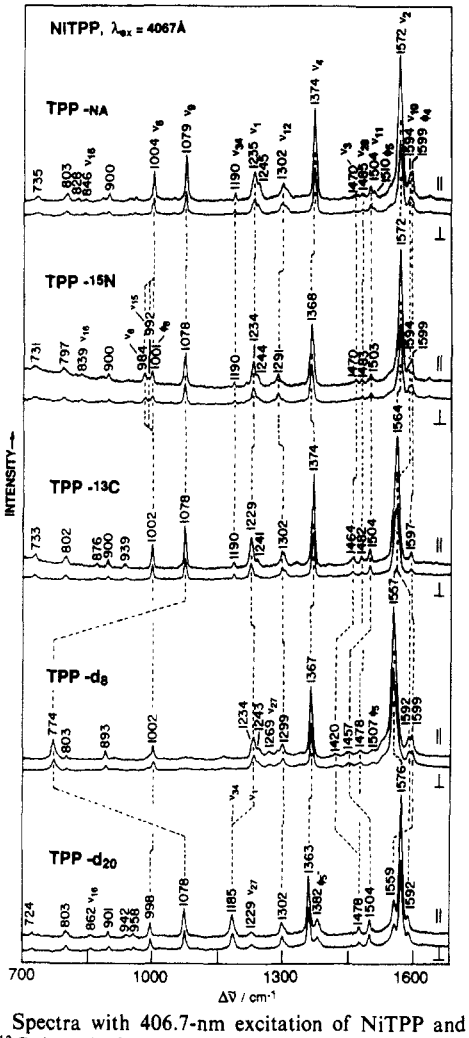

Figure 9. Spectra with 406.7-nm excitation of NiTPP and its $^{15}N_4$ (pyrrole), $^{13}C_4$ (meso), d_8 (pyrrole), and d_{20} (phenyl) isotopomers, in KCl pellets. Conditions: 150 mW laser power, 4 cm^{-1} slit widths.

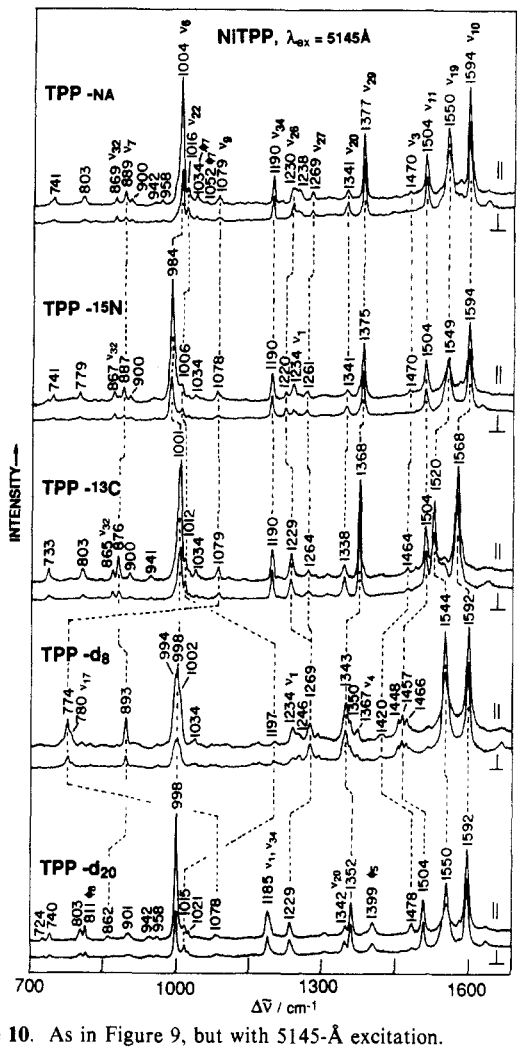

Figure 10. As in Figure 9, but with 5145-Å excitation.

contains ~10% of the absorption strength of the B band.

In resonance with the B band (406.7 nm excitation, Figures 5 and 9) the RR spectrum is dominated by polarized bands (p) arising from totally symmetric modes, A_{1g}. The symmetric modes are enhanced via *A* term (Franck–Condon) scattering, the dominant mechanism for resonance with strongly allowed electronic transitions.[30,31] The *A* term scales with the square of the electronic transition moment and is much weaker for Q than for B band resonance. Nevertheless, polarized bands are seen in Q-band-excited spectra (Figures 6, 10, and 11), since the Q_0 absorption strength, ~10% of the B band strength for NiP, is not negligible. Interestingly, the intensity pattern of the polarized bands is quite different for B and Q resonance, implying marked differences in the Franck–Condon factors. Thus the high-frequency bands ν_2 and ν_4 dominate the 406.7-nm-excited spectrum but have negligible intensity in the 530.9-nm (NiP, Figure 6) or 514.5-nm (NiTPP, Figure 10) spectra, where ν_6 and ν_7 are the strongest polarized bands. The reversal in intensities implies a reversal in relative magnitudes of the Franck–Condon products for the high- and mid-frequency modes, indicating quite different shapes for the B and Q excited-state potentials.

Most of the bands in the 514.5-, 530.9-, and 568.2-nm spectra are depolarized (dp) and anomalously polarized (ap). They arise from B_{1g} or B_{2g} (dp) and A_{2g} (ap) modes which are vibronically active in Q–B mixing. They are enhanced via the B (vibronic) term,[30,31] and their intensities depend on the vibronic coupling strengths of the individual modes. Still another scattering mechanism involves Jahn–Teller activity,[32] since the B and Q excited states are both degenerate. B_{1g} and B_{2g}, but not A_{2g}, modes can be enhanced via the Jahn–Teller effect. This is the likely source of the depolarized band activation (ν_{10}, ν_{11}, ν_{13}) in the 406.7-nm spectra.

4. NiP. Excitation at 406.7 and 530.9 nm (Figures 5 and 6) exposes all the Raman-active fundamental bands above 700 cm^{-1} for NiP. At lower frequencies a single wavelength is sufficient to display the fundamental bands: 514.5 nm for the 650–850-cm^{-1} region (Figure 7) and 530.9 nm for the 150–650-cm^{-1} region (Figure 8). Infrared spectra were also obtained (not shown) in the 450–1700-cm^{-1} region.

Table IV gives the assignments of the RR and infrared bands according to the local coordinate scheme discussed above, while Table V gives observed and calculated frequencies and isotope shifts. All of the NiP in-plane fundamentals have now been assigned, with the exception of the CH stretches, expected in the 3000-cm^{-1} region. The assignments are based on the frequency ordering of the bands and their sensitivities to deuteration at the meso (d_4) and pyrrole (d_8) positions. Thus the highest frequency bands (excluding the C–H stretches, calculated near 3000 cm^{-1}), are between 1450 and 1660 cm^{-1} and are assigned to stretching modes of the shortest bonds,[25] $C_\beta C_\beta$ and $C_\alpha C_m$, based on their relative d_8 (substitution on C_β's) and d_4 (substitution on C_m's) shifts. There is ambiguity between the ν_2 and ν_3 assignments in the A_{1g} block, since the 1574- and 1459-cm^{-1} bands both show larger d_8 than d_4 shifts, indicating substantial coordinate mixing. The d_8 shift, along with the calculated $C_\beta C_\beta$ contributions to the

(30) Tang, J.; Albrecht, A. C. In *Raman Spectroscopy*; Szymanski, H. A., Ed.; Plenum Press: New York, 1970; Vol. II, p 33.
(31) Spiro, T. G.; Stein, P. *Annu. Rev. Phys. Chem.* **1977**, *28*, 501.
(32) (a) Cheung, L. D.; Yu, N.-T.; Felton, R. H. *Chem. Phys. Lett.* **1978**, *55*, 527. (b) Shelnutt, J. A.; Cheung, L. D.; Cheng, C. C.; Yu, N.-T.; Felton, R. H. *J. Chem. Phys.* **1977**, *66*, 3387.

TABLE IV: Allocation of NiP Skeletal Mode Frequencies (cm^{-1}) to Local Coordinates[a]

local coordinate	A_{1g}	B_{1g}	A_{2g}	B_{2g}	E_u
$\nu(C_mH)$	ν_1 [3042]			ν_{27} [3041]	ν_{36} [3042]
$\nu(C_\alpha C_m)_{asym}$		ν_{10} 1650	ν_{19} 1611		ν_{37} 1624
$\nu(C_\beta C_\beta)$	ν_2 1574	ν_{11} 1505			ν_{38} 1547
$\nu(C_\alpha C_m)_{sym}$	ν_3 1459			ν_{28} 1505	ν_{39} 1462
ν(Pyr quarter-ring)			ν_{20} 1354	ν_{29} 1368	ν_{40} 1385
ν(Pyr half-ring)$_{sym}$	ν_4 1376	ν_{12} [1319]			ν_{41} 1319
$\delta(C_mH)$		ν_{13} 1185	ν_{21} 1139		ν_{42} 1150
$\nu(C_\beta H)_{sym}$	ν_5 [3097]	ν_{14} [3097]			ν_{43} [3097]
ν(Pyr half-ring)$_{asym}$			ν_{22} 1005	ν_{30} 1003	ν_{44} 1033
$\nu(C_\beta H)_{asym}$			ν_{23} [3087]	ν_{31} [3088]	ν_{45} [3087]
δ(Pyr def)$_{asym}$			ν_{24} 806	ν_{32} 819	ν_{46} 806
ν(Pyr breathing)	ν_6 995	ν_{15} 1003			ν_{47} 995
δ(Pyr def)$_{sym}$	ν_7 732	ν_{16} 732			ν_{48} 745
δ(Pyr rot.)			ν_{25} 429	ν_{33} 435	ν_{49} 366
ν(NiN)	ν_8 369	ν_{18} 237			ν_{50} 420
$\delta(C_\beta H)_{asym}$			ν_{26} 1317	ν_{34} 1185	ν_{51} 1250
$\delta(C_\beta H)_{sym}$	ν_9 1066	ν_{17} 1060			ν_{52} 1064
δ(Pyr transl)				ν_{35} 197	ν_{53} 282

[a] Observed frequencies from CS_2 solution RR (A and B modes) and KBr pellet IR (E modes) spectra. Numbers in square brackets are calculated values.

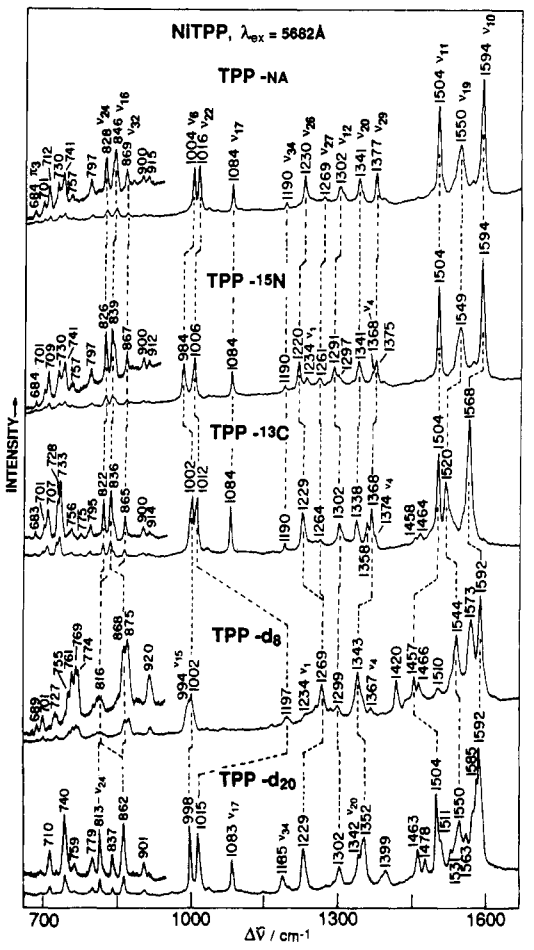

Figure 11. As in Figure 9, but with 5682-Å excitation; inset of 700–900-cm^{-1} region with expanded scale (several bands in this region are assigned to out-of-plane modes, see ref 14b).

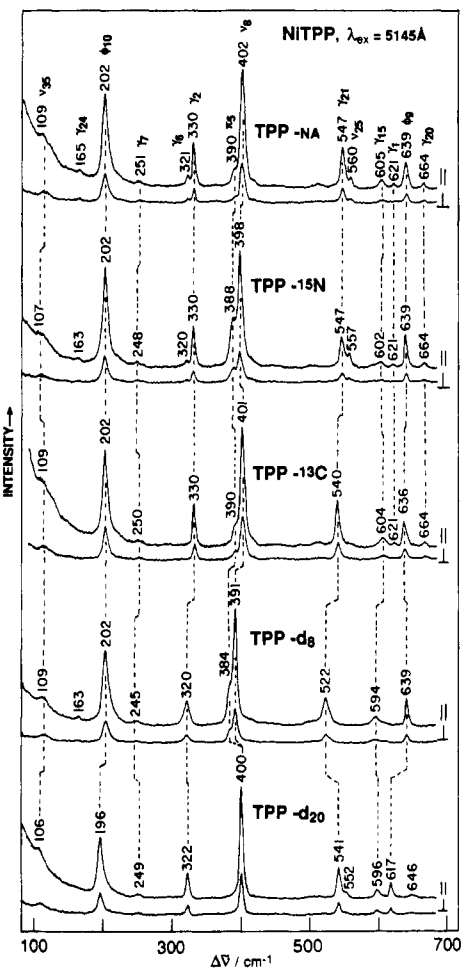

Figure 12. As in Figure 9, but 80–680-cm^{-1} region, with 5145-Å excitation.

potential energy distribution, is somewhat larger for the 1459- than the 1575-cm^{-1} band, suggesting a preferred $C_\beta C_\beta$ (ν_2) assignment for the former. Nevertheless, the higher of the two bands is listed as ν_2 in conformity with NiOEP,[3] for which the $\nu(C_\beta C_\beta)/\nu(C_\alpha C_m)$ mixing is much smaller.[14a] This mode mixing is the likely reason for the anomalously low intensity of the ν_3 band in the 406.7-nm-excited spectrum. Due to the phasing of the mixed coordinates, the intensity adds up for ν_2, the strongest band in the spectrum, and nearly cancels for ν_3. By contrast ν_2 and ν_3 are equally strong in the 406.7-nm-excited spectrum of NiOEP,[14a] consistent with the reduced mixing.

A cleaner separation of $C_\beta C_\beta$ and $C_\alpha C_m$ stretching is seen in the B_{1g} and E_u blocks ($C_\beta C_\beta$ does not contribute to A_{2g} or B_{2g}) since ν_{11} and ν_{38} ($\nu(C_\beta C_\beta)$) have much larger d_8 than d_4 shifts, and vice versa for ν_{10}, ν_{37}, and ν_{39} ($\nu(C_\alpha C_m)$). The large frequency difference between asymmetric and symmetric $C_\alpha C_m$ modes (cf. 160 cm^{-1} between ν_{37} and ν_{39}) reflects the kinematic interaction at the relatively large (121.4°) $C_\alpha C_m C_\alpha$ angle, as well as the positive 1,2 interaction force constant between the $C_\alpha C_m$ bond stretches.

The trio of pyrrole quarter-ring stretches are assigned at 1354 (A_{2g}), 1368 (B_{2g}), and 1385 (E_u) cm^{-1}, based on the frequency

TABLE V: Observed and Calculated Frequencies (cm^{-1}) for NiP and Its Isotopomers[a]

	NA			d_4		d_8		d_{12}	
ν_i	obsd	calcd ($\Delta^{15}N$)[b]	assignment (PED, %)[c]	obsd	calcd	obsd	calcd	obsd	calcd
			A_{1g} Modes						
ν_5		3097 (0)	$\nu(C_\beta H)$ (99)		3097		2319		2319
ν_1		3042 (0)	$\nu(C_m H)$ (99)		2272		3042		2272
ν_2	1574	1564 (0)	$\nu(C_\beta C_\beta)$ (41) + $\nu(C_\alpha C_m)$ (22)	1566	1558	1552	1543	1546	1533
ν_3	1459	1459 (0)	$\nu(C_\alpha C_m)$ (32) + $\nu(C_\beta C_\beta)$ (35)	1456	1446	1431	1440	1427	1429
ν_4	1376	1384 (2)	$\nu(C_\alpha C_\beta)$ (43) + $\nu(NC_\alpha)$ (22)	1374	1382	1367	1361	1367	1361
ν_9	1066	1079 (1)	$\nu(C_\beta H)$ (78) + $\nu(C_\alpha C_\beta)$ (12)	1065	1077	775	782	773	781
ν_6	995	1020 (20)	$\nu(C_\alpha C_\beta)$ (29) + ν(NCa) (16) + ν(NiN) (11)	992	1017	987	1014	985	1011
ν_7	732	725 (0)	$\delta(C_\alpha C_m C_\alpha)$ (29) + $\nu(NC_\alpha)$ (22) + $\delta(C_\alpha C_m)$ (14)	711	705	720	721	709	701
ν_8	369	378 (2)	ν(NiN) (27) + $\nu(C_\alpha C_m)$ (27)	367	377	360	371	359	370
			B_{1g} Modes						
ν_{14}		3097 (0)	$\nu(C_\beta H)$ (99)		3097		2318		2318
ν_{10}	1650	1649 (0)	$\nu(C_\alpha C_m)$ (85) + $\delta(C_\alpha C_m H)$ (10)	1642	1641	1646	1646	1636	1638
ν_{11}	1505	1529 (0)	$\nu(C_\beta C_\beta)$ (70) + $\delta(C_\beta H)$ (22)	1504	1529	1454	1488	1454	1487
ν_{12}		1319 (11)	$\nu(NC_\alpha)$ (56) + $\nu(C_\alpha C_\beta)$ (21)	1321	1309	1324	1309	1315	1293
ν_{13}	1185	1197 (1)	$\delta(C_m H)$ (70) + $\nu(C_\alpha C_\beta)$ (13)	938	937	1179	1187	948	935
ν_{17}	1060	1064 (0)	$\delta(C_\beta H)$ (75) + $\nu(C_\beta C_\beta)$ (16)		1066	768	778	768	777
ν_{15}	1003	1015 (14)	$\nu(C_\alpha C_\beta)$ (53) + $\nu(NC_\alpha)$ (12)	1020	1042		996		1021
ν_{16}	732	710 (3)	$\delta(C_\alpha C_\beta C_\beta)$ (23) + $\delta(NC_\alpha C_\beta)$ (17) + $\nu(C_\alpha C_m)$ (14) + $\delta(C_\alpha C_m)$ (14)	665	634	705	709	655	634
ν_{18}	237	245 (1)	ν(NiN) (64) + $\delta(C_\alpha C_m)$ (33)	237	245	232	241	232	241
			A_{2g} Modes						
ν_{23}		3087 (0)	$\nu(C_\beta H)$ 100		3087		2298		2298
ν_{19}	1611	1602 (2)	$\nu(C_\alpha C_m)$ (89) + $\nu(NC_\alpha)$ (12)	1598	1593	1605	1601	1592	1592
ν_{20}	1354	1351 (1)	$\nu(C_\alpha C_\beta)$ (47) + $\delta(C_\beta H)$ (48) + ν(NC)α) (11)	1347	1351	1313	1321	1278	1298
ν_{26}	1317	1319 (8)	$\delta(C_m H)$ (34) + $\delta(C_\beta H)$ (25)	1249	1279	851	855	848	852
ν_{21}	1139	1120 (1)	$\delta(C_m H)$ (48) + $\delta(C_\beta H)$ (16) + $\nu(C_\alpha C_\beta)$ (19)	910	865	1256	1231	848	859
ν_{22}	1005	992 (4)	$\nu(NC_\alpha)$ (35) + $\nu(C_\alpha C_\beta)$ (20)	1012	1016	1095	1070	1189	1187
ν_{24}	806	796 (0)	$\delta(C_\alpha C_\beta C_\beta)$ (33) + $\delta(NC_\alpha C_\beta)$ (22) + $\nu(C_\alpha C_\beta)$ (14)	783	762	788	777	767	750
ν_{25}	429	416 (1)	$\delta(C_\alpha C_m)$ (116)	419	412	404	399	397	392
			B_{2g} Modes						
ν_{31}		3088 (0)	$\nu(C_\beta H)$ (99)		3088		2299		2300
ν_{27}		3041 (0)	$\nu(C_m H)$ (99)		2269		3041		2268
ν_{28}	1505	1492 (6)	$\nu(C_\alpha C_m)$ (41) + $\nu(NC_\alpha)$ (43)	1477	1480	1487	1483	1481	1470
ν_{29}	1368	1381 (0)	$\nu(C_\alpha C_\beta)$ (58) + $\nu(C_\beta H)$ (40)	1368	1381	1324	1326	1315	1326
ν_{34}	1193	1183 (0)	$\delta(C_\beta H)$ (52) + $\nu(C_\alpha C_\beta)$ (21)	1193	1182		965	948	959
ν_{30}		1036 (19)	$\nu(NC_\alpha)$ (42) + $\nu(C_\alpha C_m)$ (14) + $\delta(C_\alpha C_m)$ (15)	1020	1017		1050		1034
ν_{32}	819	836 (0)	$\delta(C_\alpha C_\beta C_\beta)$ (42) + $\delta(C_\alpha C_m C_\alpha)$ (25)	815	828	799	787	780	782
ν_{33}	435	424 (0)	$\delta(C_m C_\alpha)$ (30) + $\nu(C_\alpha C_m)$ (22) + $\delta(C_\alpha C_\beta)$ (16)	432	424	399	389	399	389
ν_{35}	197	202 (2)	$\delta(C_\alpha$NNi) (42) $\delta(C_\alpha C_m C_\alpha)$ (23)	197	200	197	201	197	199
			E_u Modes						
ν_{43}		3097 (0)	$\nu(C_\beta H)$ (99)		3097		2319		2319
ν_{45}		3088 (0)	$\nu(C_\beta H)$ (99)		3088		2298		2299
ν_{36}		3042 (0)	$\nu(C_m H)$ (99)		2270		3042		2270
ν_{37}	1624	1628 (1)	$\nu(C_\alpha C_m)$ (87) + $\delta(C_m H)$ (10)	1620	1620	1624	1626	1628	1618
ν_{38}	1547	1550 (1)	$\nu(C_\beta C_\beta)$ (49) + $\nu(C_\alpha C_m)$ 15 + $\delta(C_\beta H)$ (18)	1543	1545	1527	1523	1520	1515
ν_{39}	1462	1472 (5)	$\nu(C_\alpha C_m)$ (32) + $\nu(NC_\alpha)$ (30) + $\nu(C_\beta C_\beta)$ (23)	1458	1460	1420	1452	1420	1442
ν_{40}	1385	1379 (12)	$\nu(C_\alpha C_\beta)$ (53) + $\delta(C_\beta H)$ (32) + $\nu(NC_\alpha)$ (11)	1373	1378		1342		1340
ν_{41}	1319	1338 (10)	$\nu(NC_\alpha)$ (45) + $\nu(C_\alpha C_\beta)$ (30)	1315	1331	1265	1315	1265	1299
ν_{52}	1250	1272 (2)	$\delta(C_m H)$ (32) + $\delta(C_\beta H)$ (29) + $\nu(NC_\alpha)$ (10) + $\nu(C_\alpha C_\beta)$ (10)	910	900	1192	1209	945	903
ν_{42}	1150	1138 (2)	$\delta(C_m H)$ (42) + $\delta(C_\beta H)$ (21)	1261	1234	914	903	860	891
ν_{51}	1064	1074 (1)	$\delta(C_\beta H)$ (74) + $\nu(C_\beta C_\beta)$ (13)	1068	1074	794	779	764	775
ν_{44}	1033	1012 (13)	$\nu(C_\alpha C_\beta)$ (39) + $\nu(NC_\alpha)$ (20) + $\delta(C_b H)$ (10)	1026	1030	1091	1065	1123	1134
ν_{47}	995	1003 (20)	$\nu(NC_\alpha)$ (34) + $\nu(C_\alpha C_\beta)$ (14)	999	998	983	998	998	991
ν_{46}	806	820 (1)	$\delta(C_\beta C_\beta C_\alpha)$ (37) + $\delta(NC_\alpha C_\beta)$ (14) + $\delta(C_\alpha C_m C_\alpha)$ (18) + $\nu(NC_\alpha)$ (11)		807		794		783
ν_{48}	745	722 (1)	$\delta(NC_\alpha C_\beta)$ (18) + $\delta(C_\alpha C_m)$ (19) + $\nu(NC_\alpha)$ (12)	648	664	737	704	648	654
ν_{50}	420	413 (2)[d]	ν(NiN) (50) + $\nu(C_\alpha C_m)$ (19)		411		403		401
ν_{49}	366	352 (3)	$\delta(C_\alpha C_m)$ (78) + $\delta(C_\alpha$NNi) (17)		349		336		333
ν_{53}	282	281 (0)[d]	ν(NiN) (44) + δ(NNiN) (10) + δ (C_αNNi) 10		280		277		276

[a] Observed frequencies from CS_2 solution (A and B modes) RR and KBr pellet IR (E modes) spectra at room temperature. NA = natural abundance; d_4, d_8, d_{12} = ^{2}H-substituted analogues at the C_m, C_β, and $C_m + C_\beta$ positions, respectively. [b] Calculated isotope shifts (cm^{-1}) upon ^{15}N substitution at the pyrrole nitrogens shown in parentheses; observed values not available. [c] PED = potential energy distribution (%). [d] Calculated $^{62/58}$Ni isotope shifts are 2.2 and 4.8 cm^{-1} for ν_{50} and ν_{53}, respectively.

order in the respective symmetry blocks and on the sensitivity (40–50 cm^{-1}) to pyrrole deuteration. In the A_{2g} block, extensive mixing between the quarter ring stretch (ν_{20}, 1354 cm^{-1}) and the $C_\beta H$ bending mode (ν_{26}, 1317 cm^{-1}) again results in a large intensity disparity, almost all of the intensity appearing in ν_{26}. The ν_{20} mode regains substantial intensity in the spectra of the d_8 species, as ν_{26} shifts down and the interaction is lifted.

The strong polarized band at 1376 cm^{-1}, ν_4, is assigned to the A_{1g} pyrrole symmetric half-ring stretch. In the context of the NiOEP spectrum, this band has been assigned[3] to the $C_\alpha N$ breathing mode, on the basis of its ^{15}N shift (this shift is unavailable for porphine), but the 9-cm^{-1} d_8 shift in NiP supports the involvement of the entire pyrrole ring. The corresponding B_{1g} mode, ν_{12}, is not detected in the natural abundance spectrum, but

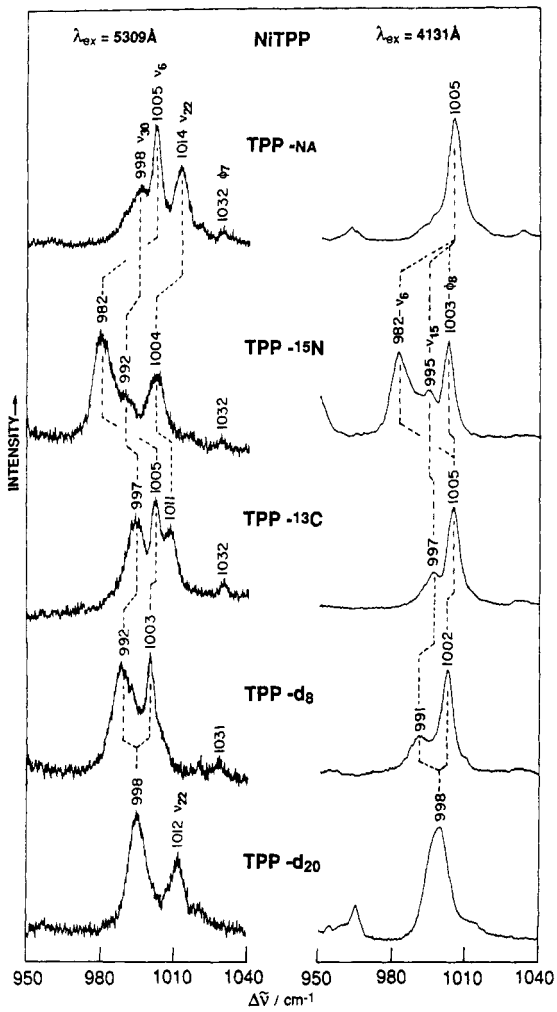

Figure 13. Details of the 950–1050-cm^{-1} RR spectra of NiTPP in CS_2 with 5309-Å (left panel) and 4131-Å (right panel) excitation.

weak bands at ~1322 cm^{-1} in the d_4 and d_8 spectra are assignable to this mode (see Table V). The E_u counterpart (ν_{41}) is seen at 1319 cm^{-1} in the IR spectrum. The asymmetric half-ring stretches are at much lower frequency, 1003–1033 cm^{-1}, reflecting the large kinematic effect of the phasing of the bond stretches. The pyrrole breathing modes are all at ~1000 cm^{-1}, close to the corresponding mode of pyrrole itself;[24] likewise the symmetric and asymmetric five-membered ring pyrrole deformations at ~735 and ~810 cm^{-1} are close to those of free pyrrole.[24] All of the CH bending modes are in the 1050–1200-cm^{-1} region, except for the A_{2g} $C_\beta H$ bending mode, ν_{26} (1317 cm^{-1}), which is heavily mixed with the C_mH bending mode (ν_{21}, 1139 cm^{-1}) of the same symmetry. This mixing is reflected in the strong down- and upshifts of these modes upon pyrrole deuteration (Table V). In the d_4 spectrum the downshifted ν_{26} (~1250 cm^{-1}) appears to split into four ap bands, presumably due to Fermi resonance with combination modes of A_{2g} symmetry in the meso-deuterated species.

We remark on the intensity of ν_9 at 1066 cm^{-1}, which is assigned to $C_\beta H$ bending. Bending coordinates are not generally considered to be important contributors to the Raman intensity, but ν_9 is the third strongest band in the 406.7-nm-excited spectrum (Figure 5). Although there is some mixing between ν_9 and ν_6, the pyrrole breathing mode, the intensity cannot be explained on this basis since the ν_6 intensity actually *decreases* in the spectrum of the d_8 isotopomer, when the $\delta(C_\beta H)$ coordinate is shifted out of the region. Thus substantial intensity is allocable directly to $\delta(C_\beta H)$, implying that there is a significant change in the $C_\beta C_\beta H$ angle in the excited state. The other CH bending coordinate, $\delta(C_mH)$, does not contribute to the A_{1g} block, and there can be no change in the $C_\alpha C_mH$ angle upon excitation without symmetry lowering. The Jahn–Teller effect, which gives rise to B_{1g} or B_{2g} enhancement, does lower the symmetry, and we note that the B_{1g} $\delta(C_mH)$ mode, ν_{13}, *does* have significant intensity in the 406.7-nm-excited spectrum.

In the low-frequency region one finds the B_{1g} NiN stretch, ν_{18}, at 237 cm^{-1}, a frequency consistent with the large effective mass of the pyrrole rings. For comparison the breathing mode frequency of the $Cu(imidazole)_4^{2+}$ complex is 245 cm^{-1}.[33] The A_{1g} and E_u counterparts, ν_8 and ν_{50}, are at much higher frequencies, 369 and 420 cm^{-1}. This elevation reflects the fact that when adjacent Ni–pyrrole bonds are stretched in phase the $C_\alpha C_m C_\alpha$ angle has to expand; consequently the force constant for the mode contains both the NiN stretching and $C_\alpha C_m C_\alpha$ bending force constants. When adjacent stretches are out-of-phase, however, as they are in the B_{1g} mode, then the $C_\alpha C_m C_\alpha$ angle is unaltered.

The pyrrole translations are at ~200 cm^{-1} while the rotations are at higher frequency, ~400 cm^{-1}. An interesting aspect of the RR spectra is the appearance of the A_{2g} pyrrole rotation, ν_{25}, as an ap band at 429 cm^{-1}. This is the lowest frequency ap band so far reported; anomalously polarized intensity is expected to go to zero as the mode frequency approaches zero, due to the negative interference in the antisymmetric Raman tensor between the 0–0 and 0–1 vibronic contributions.[31]

The many frequency correspondences in Table IV indicate that the local coordinates chosen for the classification are the primary determinants of the normal modes, the phasing among them, which determine the symmetry species, having relatively small effects on the frequencies. There are, however, significant interactions among some of the coordinates in some of the blocks, as discussed above. Because of the absence of substituent internal vibrations, porphine gives the simplest and most easily classifiable vibrational pattern of any of the porphyrins. The next step in increasing complexity is represented by tetraphenylporphine.

5. NiTPP. a. Skeletal Modes. RR spectra in the 700–1700-cm^{-1} region are shown for NiTPP in Figures 9, 10, and 11, with 406.7-, 514.5-, and 568.2-nm excitation, respectively. The latter two are near resonance with the Q_1 and Q_0 absorption bands (Figure 4) and show different enhancement patterns which help to disentangle the modes, especially in the 1000-cm^{-1} region where several bands overlap (see below). Spectra in the 80–680-cm^{-1} region are shown in Figure 12 for 514.5-nm excitation. Table VI gives assignments to the local coordinates while Table VII compares observed and calculated frequencies and isotope shifts for the NiTPP porphyrin skeletal modes. Observed and calculated phenyl modes are listed in Table VIII. In addition to these modes, the low-frequency spectra contain bands which are assigned to porphyrin out-of-plane modes. These are labeled in Figures 8 and 11, and discussed in the third paper of this series.[14b] Finally, there are a few weak bands which are assigned to overtone and combination modes, as indicated in the figures. For NiTPP we have not included infrared assignments, because the IR spectra are extremely complex due to numerous strong phenyl contributions, and correlations among the isotopomers are quite arbitrary.

A comparison of Tables IV and VI reveals a remarkably close correspondence among similarly assigned bands of NiP and NiTPP, when due allowance is made for the substitution of the C_mH bending modes of the former (~1150 cm^{-1}) with the much lower frequency C_m–phenyl bending modes of the latter (~250 cm^{-1}). The principal effect is in the A_{2g} block, where loss of the $\delta(C_mH)/\delta(C_\beta H)$ mixing in NiTPP lowers the $\delta(C_\beta H)$ mode, ν_{26}, to 1230 cm^{-1} (from 1317 cm^{-1} in NiP), closer to the other asymmetric $\delta(C_\beta H)$ mode, $\nu_{34}(B_{2g})$ at 1190 cm^{-1}. Most of the other NiTPP bands are within a few cm^{-1} of the corresponding bands in NiP. Significant exceptions are the asymmetric $C_\alpha C_m$ stretching modes, ν_{10} and ν_{19}, which are ~60 cm^{-1} lower in NiTPP than NiP. Most (~70%) of this lowering is due to the loss of the $\delta(C_mH)$ interaction, unique to the B_{1g} and A_{2g} blocks, which pushes ν_{10} and ν_{19} up. (This effect was estimated from a calculation of the NiTPP frequencies with the unaltered NiP force field.) The rest of the effect is brought about by increasing the interaction force constant for adjacent $C_\alpha C_m$ bonds (Table II),

(33) Larrabee, J. A.; Spiro, T. G. *J. Am. Chem. Soc.* **1980**, *102*, 4217–4223.

TABLE VI: Allocation of NiTPP Skeletal Mode Frequencies (cm^{-1}) to Local Coordinates[a]

local coordinate	A_{1g}	B_{1g}	A_{2g}	B_{2g}	E_u
$\nu(C_mPh)$	ν_1 1235			ν_{27} 1269	ν_{36} [1254]
$\nu(C_\alpha C_m)_{asym}$		ν_{10} 1594	ν_{19} 1550		ν_{37} [1586]
$\nu(C_\beta C_\beta)$	ν_2 1572	ν_{11} 1504			ν_{38} [1552]
$\nu(C_\alpha C_m)_{sym}$	ν_3 1470			ν_{28} 1485	ν_{39} [1473]
ν(Pyr quarter-ring)			ν_{20} 1341	ν_{29} 1377	ν_{40} [1403]
ν(Pyr half-ring)$_{sym}$	ν_4 1374	ν_{12} 1302			ν_{41} [1331]
$\delta(C_mPh)$		ν_{13} 238	ν_{21} [255]		ν_{42} [233]
$\nu(C_\beta H)_{sym}$	ν_5 [3101]	ν_{14} [3100]			ν_{43} [3100]
ν(Pyr. half-ring)$_{asym}$			ν_{22} 1016	ν_{30} 998[b]	ν_{44} [1003]
$\nu(C_\beta H)_{asym}$			ν_{23} [3096]	ν_{31} [3096]	ν_{45} [3097]
δ(Pyr def)$_{asym}$			ν_{24} 828	ν_{32} 869	ν_{46} [864]
ν(Pyr breathing)	ν_6 1004	ν_{15} 1005[b]			ν_{47} [1023]
δ(Pyr def)$_{sym}$	ν_7 889	ν_{16} 846			ν_{48} [895]
δ(Pyr rot.)			δ_{25} 560	ν_{33} 450	ν_{49} [512]
ν(NiN)	ν_8 402	ν_{18} 277			ν_{50} [436]
$\delta(C_\beta H)_{asym}$			ν_{26} 1230	ν_{34} 1190	ν_{51} [1093]
$\delta(C_\beta H)_{sym}$	δ_9 1079	ν_{17} 1084			ν_{52} [1213]
δ(Pyr transl)				ν_{35} 109	ν_{53} [306]

[a] Observed frequencies from room temperature RR spectra of crystalline NiTPP. Numbers in square brackets are calculated values. [b] These values from CS_2 solution RR spectra.

and appears to be a genuine electronic influence of the phenyl groups.

Another big effect is the ~150-cm^{-1} increase in the ν_7 and ν_{16} frequencies, assigned to symmetric pyrrole deformation, from ~730 cm^{-1} in NiP to ~840–880 cm^{-1} in NiTPP. This shift is attributable to a near-resonant interaction with phenyl deformation modes; in biphenyl, the deformation mode is at 740 cm^{-1}.[23a] The shifted phenyl modes are calculated (see next section) near 630 cm^{-1} and the A_{1g} mode appears as a polarized band at 639 cm^{-1} (Figure 12). A consequence of the strong interaction is that most of the intensity accumulates in the 639-cm^{-1} band. Indeed the assignments could equally well be reversed, but the ~639-cm^{-1} band shows a larger d_{20} frequency shift and so is allocated to the phenyl mode. A similar near-resonant interaction with a phenyl mode (ϕ_{10}, see below) accounts for the downshift of ν_{35}, from 197 cm^{-1} in NiP to 109 cm^{-1} in NiTPP.

As in the case of NiP there is heavy $\nu(C_\beta C_\beta)/\nu(C_\alpha C_m)$ mixing in the ν_2 and ν_3 modes resulting in a marked intensity disparity; again ν_2 is assigned to the higher frequency band, in conformity with NiOEP.

The present assignments of the NiTPP skeletal modes are in general consistent with (but more complete than) those of Stein et al.,[9] based on d_8 and d_{20} isotope shifts in $(FeTPP)_2O$,[8] as amended slightly by Parthasarathi et al.,[34] who examined the core size dependency of the skeletal modes for several metallo-TPP's. However, their assignment of a mode lying slightly higher than ν_4 to a B_{1g} mode[34] seems to be incorrect, since the closest B_{1g} mode, ν_{12}, is calculated at an appreciably lower frequency, corresponding to a weak band at 1302 cm^{-1} in NiTPP. The band close to ν_4 is the B_{2g} mode ν_{29}, at 1377 cm^{-1} in NiTPP. The ν_{29} and ν_{12} modes (both of which give rise to depolarized bands) are readily distinguished by the small ^{15}N and large d_8 shifts for ν_{29}, but large ^{15}N and small d_8 shifts for ν_{12} (see Table VII).

We remark on the complexity of the 1000-cm^{-1} region of the NiTPP RR spectra. The pyrrole breathing modes ν_6 and ν_{15} as well as the asymmetric half-ring stretches ν_{22} and ν_{30} and a phenyl mode, ϕ_8, all lie within a few cm^{-1}. These can nevertheless be sorted out by the differing polarizations and excitation wavelength dependencies as well as the isotope shifts, as shown in Figure 13. Thus with 5309-Å excitation ν_6 (1005 cm^{-1}, p) is resolved from the flanking bands ν_{22} (1014 cm^{-1}, ap) and ν_{30} (998 cm^{-1}, dp), but with 4131-Å excitation a single 1005-cm^{-1} band is observed, which resolves into three bands upon ^{15}N substitution: ν_6 (982 cm^{-1}, p), ν_{15} (995 cm^{-1}) dp, and ϕ_8 (1003 cm^{-1}, p). These spectra were obtained in CS_2 solution to be certain of the depolarization ratios, and the frequencies differ slightly from those obtained in KCl pellets, which are reported in the preceding figures and the tables.

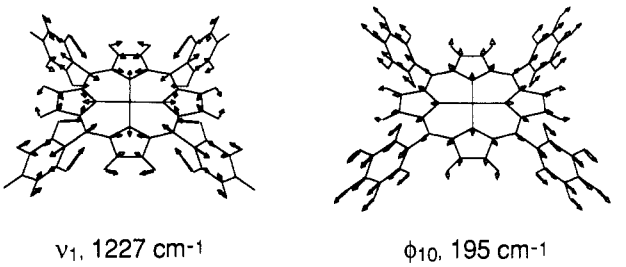

Figure 14. Eigenvectors for the two A_{1g} modes which involve C_m–phenyl stretching. The left one is allocated to ν_1 and the right one to a phenyl mode.

b. Phenyl Modes. Phenyl modes can readily be identified via their d_{20} shifts. Stein et al.[9] catalogued several of these by comparison with biphenyl, which serves as a useful model. We have calculated all of the phenyl modes which transform as the porphyrin in-plane skeletal modes, and have tabulated them in Table VIII, along with observed frequencies. Since the phenyl rings are perpendicular to the porphyrin plane, coordinates can contribute which are out of the phenyl planes as well as those which are in the phenyl planes. The former contribute to the B_{1g}, A_{2g}, and E_u blocks, while the latter contribute to the A_{1g}, B_{2g}, and E_u blocks. Only those phenyl coordinates contribute which are symmetric with respect to the porphyrin plane; the antisymmetric ones (half the total), contribute to the out-of-plane porphyrin modes. Phenyl modes involving a given phenyl coordinate fall at nearly the same frequency, regardless of the symmetry block, since the phenyl groups interact very little with one another. Consequently Table VIII is arranged in nearly isofrequency triplets. The in-(phenyl)plane modes are labeled ϕ_i, ϕ_i', ϕ_i'' corresponding to the A_{1g}, B_{1g}, and E_u modes, respectively, while the out-of-(phenyl)plane modes are labeled π_i, π_i', and π_i'', corresponding to the B_{1g}, A_{2g}, and E_u modes. For each triplet the Wilson notation (ν_i) for phenyl modes is also given to identify the coordinate involved.[35]

As noted by Stein et al.,[9] there is an ambiguity about how to classify modes involving the stretching of the inter-ring bond C_m–Ph. This coordinate is a major contributor to two triplets of modes with very different frequencies: ~1250 and ~200 cm^{-1} (1285 and 315 cm^{-1} in biphenyl[23a]). In the lower frequency modes the phenyl atoms move in the same direction as the C_m–Ph bond stretch, while in the higher frequency mode the C_m–Ph bond stretch is opposed by the phenyl motion. This is clearly shown

(34) Parthasarathi, N.; Hansen, C.; Yamaguchi, S.; Spiro, T. G. *J. Am. Chem. Soc.* **1987**, *109*, 3865.

(35) Dollish, F. R.; Fateley, W. G.; Bentley, F. F. *Characteristic Raman Frequencies of Organic Compounds*; Wiley-Interscience: New York, 1974; Chapter 13.

TABLE VII: Observed and Calculated Skeletal Mode Frequencies (cm^{-1}) for NiTPP and Its Isotopomers[a]

	NA			$^{13}C_4$		d_8		d_{20}	
ν_i	obsd ($\Delta^{15}N$)	calcd ($\Delta^{15}N$)	assignment (PEP, %)[b]	obsd	calcd	obsd	calcd	obsd	calcd
			A_{1g} Skeletal Modes						
ν_5		3101 (0)	$\nu(C_\beta H)$ (99)		3101		2326		3101
ν_2	1572 (0)	1573 (0)	$\nu(C_\alpha C_m)$ (29) + $\nu(C_\beta C_\beta)$ (15) + $\nu(CC)_{Ph}$ (18)	1564	1563	1557	1562	1576	1589
ν_3	1470 (0)	1471 (0)	$\nu(C_\beta C_\beta)$ (44) + $\nu(C_\alpha C_m)$ (19) + $\delta(CCH)_{Ph}$ (11)	1464	1464	1420	1433	1478	1480
ν_4	1374 (6)	1378 (9)	$\nu(C_\alpha C_\beta)$ (42) + $\nu(NC_\alpha)$ (21) + $\delta(C_\alpha NC_\alpha)$ (18) + $\delta(C_\alpha C_m)$ (18)	1374	1376	1367	1368	1363	1372
ν_1	1235 (1)[c]	1227 (3)	$\delta(C_mPh)$ (37) + $\nu(NC_\alpha)$ (19) + $\nu(CC)_{Ph}$ (12) + $\delta(CCH)_{Ph}$ (21)	1229	1221	1234	1224	1185	1174
ν_9	1079 (1)	1097 (1)	$\delta(C_\beta H)$ (64) + $\nu(C_\beta C_\beta)$ (10)	1078	1097	774	786	1078	1088
ν_6	1004 (20)	1006 (13)	$\nu(C_\alpha C_\beta)$ (27) + $\nu(NC_\alpha)$ (93) + $\nu(CC)_{Ph}$ (22)	1002	1005	1002	1009	998	1004
ν_7	889 (2)[d]	875 (1)	$\delta(CC)_{Ph}$ (27) + $\nu(CC)_{Ph}$ (16) + $\nu(C_\alpha C_\beta)$ (11)	876	864	893	872	862	859
ν_8	402 (4)	403 (3)	$\nu(NiN)$ (24) + $\delta(C_\alpha C_m C_\alpha)$ (16) + $\nu(C_\alpha C_m)$ (13)	401	403	391	398	400	402
			B_{1g} Skeletal Modes						
ν_{14}		3100 (0)	$\nu(C_\beta H)$ (99)		3100		2325		3100
ν_{10}	1594 (0)	1607 (1)	$\nu(C_\alpha C_m)$ (87) + $\delta(C_\alpha C,mPh)$ (7)	1568	1576	1592	1603	1592	1607
ν_{11}	1504 (0)	1505 (0)	$\nu(C_\beta C_\beta)$ (67) + $\delta(C_\beta H)$ (26)	1504	1505	1457	1452	1504	1505
ν_{12}	1302 (11)	1308 (15)	$\nu(NC_\alpha)$ (64) + $\nu(C_\alpha C_\beta)$ (21)	1302	1307	1299	1299	1303	1308
ν_{17}	1084 (0)	1088 (0)	$\delta(C_\beta H)$ (64) + $\nu(C_\beta C_\beta)$ (16) + $\nu(C_\alpha C_\beta)$(11)	1084	1088	780	783	1082	1088
ν_{15}	1005 (10)[e]	1021 (5)	$\nu(C_\alpha C_\beta)$ (57) + $\nu(NC_\alpha)$ (14)	997[e]	1016	991[e]	1014	998[e]	1021
ν_{16}	846 (7)	900 (7)	$\delta(C_\alpha NC_\alpha)$ (14) + $\gamma(CH)_{Ph}$ (21) + δ ($NC_\alpha C_\beta$) (15) + $\delta(C_\alpha C_m Ph)$ (19)	836	893	868	900	862	888
ν_{18}	277 (0)	256 (1)	$\nu(NiN)$ (53) + $\delta(C_\alpha C_m)$ (28) + $\gamma(C_m C_{Ph})$ (9)	277	256	266	252	276	255
ν_{13}	238 (0)[f]	235 (0)	$\gamma(C_m C_{Ph})$ (25) + $\tau(CC)_{Ph}$ (42)	238	235	237	235	221	206
			A_{2g} Skeletal Modes						
ν_{23}		3096 (0)	$\nu(C_\beta H)$ (99)		3096		2309		3096
ν_{19}	1550 (1)	1540 (0)	$\nu(C_\alpha C_m)$ (100) + $\nu C_\alpha C_m C_{Ph}$) (8)	1520	1508	1544	1539	1550	1540
ν_{20}	1341 (0)	1348 (0)	$\nu(C_\alpha C_\beta)$ (31) + $\delta(C_\beta H)$ (71)	1338	1347	875	868	1342	1348
ν_6	1230 (10)	1239 (10)	$\nu(NC_\alpha)$ (74) + $\nu(C_\alpha C_\beta)$ (16) + $\delta(C_\alpha C_\beta C_\beta)$ (11) + $\delta(C_\alpha C_m)$ (11)	1229	1235	1269	1250	1229	1239
ν_{22}	1016 (10)	1018 (9)	$\nu(C_\alpha C_\beta)$ (38) + $\nu(NC_\alpha)$ (23) + $\delta(C_\beta H)$ (22)	1012	1015	1197	1184	1015	1018
ν_{24}	828 (2)	818 (2)	$\delta(C_\alpha C_\beta C_\beta)$ (27) + $\delta(NC_\alpha C_b)$ (15) + $\nu(NC_\alpha)$ (12) + $\gamma(CH)_{Ph}$ (16)	822	813	816	798	813	825
ν_{25}	560 (3)	565 (4)	$\delta(C_\alpha C_m Ph)$ (33) + $\delta(C_\alpha C_m)$ (21) + $\gamma(CH)$ (14) + $\nu(C_\alpha C_m)$ (11)	560	565	554	557	511	526
ν_{21}		257 (0)[g]	$\tau(CC)_{Ph}$ (52) + $\gamma(C_{Ph}C_m)$ (21) + $\delta(C_\alpha C_m)$ (13) + $\delta(C_\alpha C_m C_{Ph})$ (9)		257		254		224
			B_{2g} Skeletal Modes						
ν_{31}		3096 (0)	$\nu(C_\beta H)$ (99)		3096		2311		3096
ν_{28}	1485 (2)	1481 (1)	$\nu(C_\alpha C_m)$ (35) + $\nu(NC_\alpha)$ (15) + $\nu(CC)_{Ph}$ (11) + $\delta(CCH)_{Ph}$ (26)	1482	1471	1478	1474	1478	1499
ν_{29}	1377 (2)	1368 (0)	$\nu(C_\alpha C_\beta)$ (43) + $\delta(C_\beta H)$ (48) + $\delta(C_\alpha C_\beta)$ (10)	1368	1365	1343	1299	1352	1361
ν_{27}	1269 (8)[h]	1267 (9)	$\nu(C_mPh)$ (31) + $\nu(NC_\alpha)$ (40) + $\delta(CH)_{Ph}$ (13)	1264	1257	1268	1262	1229	1229
ν_{34}	1190 (0)	1169 (0)	$\delta(C_\beta H)$ (43) + $\nu(C_\alpha C_\beta)$ (31)	1190	1169		975	1185	1167
ν_{30}	998 (6)[e]	1010 (5)	$\nu(CC)_{Ph}$ (62) + $\nu(NC_\alpha)$ (11)	997[e]	1008	992[e]	1013	998[e]	1002
ν_{32}	869 (2)	858 (3)	$\delta(C_\alpha C_\beta C_\beta)$ (35) + $\nu(NC_\alpha)$ (22) + $\delta(C_\alpha C_m C_\alpha)$ (14)	865	854	816	814	862	852
ν_{33}	450 (1)	427 (0)	$\delta(C_\alpha C_m)$ (31) + $\nu(C_\alpha C_m)$ (19) + $\nu(C_\alpha C_\beta)$ (16)	450	427	401	386	450	427
ν_{35}	109 (2)	112 (0)	$\delta(C_\alpha NNi)$ (32) + $\delta(C_\alpha C_m C_\alpha)$ (28) + $\delta(NNiN)$ (17)	109	111	109	11	106	109
			E_u Skeletal Modes[i]						
ν_{43}		3100 (0)	$\nu(C_\beta H)$ (99)		3100		2325		3100
ν_{45}		3097 (0)	$\nu(C_\beta H)$ (99)		3097		2312		3097
ν_{37}		1586 (1)	$\nu(C_\alpha C_m)$ (89) + $\delta(C_m C_{Ph})$ (7)		1558		1585		1588
ν_{38}		1552 (0)	$\nu(C_\alpha C_m)$ (27) + $\nu(C_\beta C_\beta)$ (19) + $\nu(CC)_{Ph}$ (13) + $\nu(NC_\alpha)$ (9)		1540		1540		1543
ν_{39}		1473 (2)	$\nu(C_\beta C_\beta)$ (29) + $\nu(C_\alpha C_m)$ (20) + $\nu(NC_\alpha)$ (12)		1463		1447		1486
ν_{40}		1403 (3)	$\nu(C_\alpha C_\beta)$ (42) + $\delta(C_\beta H)$ (27) + $\nu(NC_\alpha)$ (10) + $\delta(C_a C_m)$ (9)		1402		1370		1409
ν_{41}		1331 (7)	$\nu(C_\alpha C_b)$ (27) + $\delta(C_\beta H)$ (32) + $\nu(NC_\alpha)$ (26) + $\delta(C_\alpha C_\beta C_\beta)$ (10)		1330		1273		1331
ν_{36}		1254 (8)	$\nu(NC_\alpha)$ (41) + $\nu(C_mPh)$ (26)		1246		1244		1232
ν_52		1213 (4)	$\nu(NC_\alpha)$ (27) + $\delta(C_\alpha H)$ (23) $\nu(C_m C_{Ph})$ (8) $\nu(C_\alpha C_\beta)$ (12) + $\nu(C_m C_{Ph})$ (8)		1210		867		1189
ν_{51}		1093 (1)	$\delta(C_\beta H)$ (59) + $\nu(C_\beta C_\beta)$ (10)		1093		783		1085
ν_{47}		1023 (5)	$\nu(CC)_{Ph}$ (36) + $\nu(C_\alpha C_\beta)$ 18 + $\nu(NC_\alpha)$ (11)		1021		1129		1030
ν_{44}		1003 (11)	$\nu(C_\alpha C_\beta)$ (37) + $\nu(CC)_{Ph}$ (19) + $\nu(NC_\alpha)$ (11)		1002		1008		998
ν_{48}		895 (2)	$\delta(CCC)_{Ph}$ (20) + $\nu(C_\alpha C_\beta)$ (9) $\delta(C_m C_{Ph})$ (9)		887		928		878
ν_{46}		864 (3)	$\delta(C_\alpha C_\beta C_\beta)$ (25) + $\nu(NC_\alpha)$ (20)		861		837		857
ν_{49}		512 (1)	$\delta(C_\alpha C_m Ph)$ (23) + $\gamma(CH)_{Ph}$ (20) + $\tau(CC)_{Ph}$ (16)		507		511		480
ν_{50}		436 (1)	$\delta(C_\alpha C_m)$ (24) + $\nu(NiN)$ (21)		436		417		434
ν_{53}		306 (0)	$\nu(NiN)$ (32) + $\delta(C_\alpha C_m)$ (13)		306		299		313
ν_{42}		233 (0)	$\gamma(C_m C_{Ph})$ (29) + $\tau(CC)_{Ph}$ (27) + $\delta(C_\alpha C_m$ (12)		233		233		201

[a] Observed frequencies from crystalline NiTPP RR spectra (A and B modes). NA = natural abundance molecule; ($\Delta^{15}N$) = isotope shifts (cm^{-1}) upon pyrrole-^{15}N substitution. $^{13}C_4$ = ^{13}C substituted analogue at the methine carbons; d_8 and d_{20} = ^2H substituted analogues at the pyrrole-C_β and phenyl carbon positions, respectively. [b] PED = potential energy distribution (%). [c] See text for the discussion of porphyrin-phenyl inter-ring stretchings. [d] See text for the discussion of the porphyrin–phenyl deformation modes mixing. [e] These values from CS_2 solution RR spectra. [f] See text for the discussion of the mixing between porphyrin in-plane and phenyl out-of-plane modes. [g] Calculated A_{2g} counterpart of the ν_{13} (B_{1g}) mode. [h] Observed B_{2g} counterpart of the ν_1 (A_{1g}) mode. [i] Calculated $^{62/58}Ni$ isotope shifts (cm^{-1}): ν_{50} (1.6), ν_{53} (3.4), ν_{42} (1.1).

in the eigenvectors of the A_{1g} modes (Figure 14). Thus it is the lower frequency mode that is properly viewed as the "porphyrin–phenyl" stretch, if the phenyl group is considered as a single vibrating unit.[9] However, it is the higher frequency mode that falls in the region where C–C bond stretches are normally expected, and it gives rise to a fairly strong polarized band in the Soret-excited RR spectrum of meso-aryl-substituted porphyrins.[36] Thus we allocate the higher frequency trio as the $\nu(C_mX)$ porphyrin skeletal modes (Table VI): ν_1, ν_{27}, and ν_{36} at 1235, 1269,

(36) Blom, H.; Odo, J.; Nakamoto, K.; Strommen, D. P. *J. Phys. Chem.* **1986**, *90*, 2847.

TABLE VIII: Observed and Calculated Phenyl Modes (cm^{-1}) for NiTPP and Its Isotopomers[a]

	NA			d_8		d_{20}	
ν_i	obsd	calcd	assignments (PED, %)	obsd	calcd	obsd	calcd
			Phenyl In-Plane Modes				
ϕ_1 (ν_2)		3071	ν(CH) (99)		3071		2293
ϕ_1'		3071	ν(CH) (99)		3071		2292
ϕ_1''		3071	ν(CH) (99)		3071		2293
ϕ_2 (ν_{13})		3070	ν(CH) (99)		3070		2291
ϕ_2''	3	3070	ν(CH) (99)		3070		2291
ϕ_3 (ν_{20a})		3069	ν(CH) (99)		3069		2285
ϕ_3'		3068	ν(CH) (99)		3068		2282
ϕ_4 (ν_8a)	1599	1607	ν(CC) (61), δ(CCH) (20), $\nu(C_mC_{Ph})$ (13)	1599	1606	1559	1558
ϕ_4'		1599	ν(CC) (71), δ(CCH) (24)		1599		1572
ϕ_4''		1605	ν(CC) (67), δ(CCH) (22), $\nu(C_mC_{Ph})$ (11)		1605		1578
ϕ_5 (ν_{19a})	1510	1513	ν(CC) (29), δ(CCH) (48), $\nu(C_\beta C_\beta)$ (14)	1507	1506	1399	1400
ϕ_5'		1525	ν(CC) (30), δ(CCH) (37), $\nu(C_\alpha C_m)$ (14)		1523		1401
ϕ_5''		1513	ν(CC) (24), δ(CCH) (39), $\nu(C_\beta C_\beta)$ (23)		1498	1382	1388
ϕ_6 (ν_{9a})		1199	υ(CCH) (73), ν(CC) (13)		1199		862
ϕ_6'		1200	δ(CCH) (76), ν(CC) (12)		1200		862
ϕ_6''		1199	δ(CCH) (72), ν(CC) (12)		1200		862
ϕ_7 (ν_{18a})	1034	1037	ν(CC) (43), δ(CCH) (19)	1035	1043	811	811
ϕ_7'	1052	1063	ν(CC) (31), δ(CCH) (24), $\nu(NC_\alpha)$ (17)		1066		815
ϕ_7''		1057	ν(CC) (18), δ(CCH) (13), $\nu(NC_\alpha)$ (18)		1049		815
ϕ_8 (ν_{12})	1003	941	δ(CCC) (54), ν(CC) (28)	1002	940		912
ϕ_8		925	δ(CCC) (54), ν(CC) (17)		923		900
ϕ_8''		939	δ(CCC) (56), ν(CC) (24)		944		912
ϕ_9 (ν_{6a})	639	619	δ(CCC) (56), ν(CC) (13)	639	618	617	604
ϕ_9		631	δ(CCC) (39), ν(CC) (15), $\nu(C_mC_{Ph})$ (15)		628		613
ϕ_9''		650	δ(CCC) (45), ν(CC) (14), $\nu(C_mC_{Ph})$ (11)		646		632
ϕ_{10}, ($\nu_{Cm-\phi}$)	202	195	$\nu(C_mC_{Ph})$ (20), $\nu(C_\alpha C_m)$ (15), δ(CC) (14)	202	195	196	189
ϕ_{10}		396	δ(CCC) (29), $\nu(C_mC_{Ph})$ (15)		399		391
ϕ_{10}''		215	$\nu(C_mC_{Ph})$ (14), $\nu(C_\alpha C_m)$ (10), $\delta(C_\alpha C_m)$ (9)		213		218
			Phenyl Out-of-Plane Modes				
π_1 (ν_5)		964	γ(CH) (78), τ(CC) (51)		964		938
π_1'		961	γ(CH) (83), τ(CC) (52)		961		934
π_1''		962	γ(CH) (79), τ(CC) (52)		962		936
π_2 (ν_{17b})		823	γ(CH) (69), τ(CC) (10)		823		730
π_2'		850	γ(CH) (66), τ(CC) (12)		847		745
π_2''		827	γ(CH) (60), τ(CC) (9)		822		737
π_3 (ν_{11})	701	718	γ(CH) (86)	701	718		547
π_3'	684	718	γ(CH) (87)	689	718		563
π_3''		718	γ(CH) (87)		718		550
π_4 (ν_4)	498	474	τ(CC) (36), γ(CH) (41)	498	474		409
π_4'		441	τ(CC) (32), γ(CH) (39), $\delta(C_\alpha C_m)$ (32)		435		390
π_4''		430	τ(CC) (23), γ(CH) (30), $\delta(C_\alpha C_m)$ (9), ν(NiN) (16)		428		385
π_5 (ν_{16b})	390	388	τ(CC) (41), γ(CH) (27), $\gamma(C_{Ph}C_m)$ (15)		384	388	298
π_5'		384	τ(CC) (33), γ(CH) (18e, $\gamma(C_{Ph}C_m)$ (15), $\delta(C_\alpha C_m)$ (31)		376		302
π_5''		381	τ(CC) (30), γ(CH) (14), $\gamma(C_{Ph}C_m)$ (13), $\delta(C_\alpha C_m)$ (23)		377		287
π_6[b]		45	$\delta(C_\alpha C_m C_{Ph})$ (41), $\gamma(C_{PH}C_m)$ (40)		45		42
π_6'		83	$\delta(C_\alpha C_m C_{Ph})$ (34), $\gamma(C_{Ph}C_m)$ (51), $\delta(C_\alpha C_m)$ (12)		81		80
π_6''		49	$\delta(C_\alpha C_m C_{Ph})$ (40), $\gamma(C_{Ph}C_m)$ (40)		48		46

[a] Phenyl model notation: ϕ, ϕ', ϕ'' = modes which are in the phenyl planes phased according to A_{1g}, B_{2g}, and E_u, respectively; π, π', π'' = modes which are out of the phenyl planes phased according to B_{1g}, A_{2g}, and E_u, respectively. Wilson mode numbering (ν_i) is shown to identify the eigenvectors. Note that only those phenyl modes which are symmetric with respect to the porphyrin plane contribute to the in-plane calculation. [b] Conceited phenyl ring bendings in the porphyrin ring; see eigenvectors.

and (calc) 1254 cm^{-1}. The lower frequency trio is allocated to phenyl modes, ϕ_{10}, ϕ_{10}', and ϕ_{10}'' at (calc) 198, 396, and 215 cm^{-1}. ϕ_{10} gives rise to one of the strongest bands in the low-frequency spectrum, at 203 cm^{-1} (Figure 12). The anomalously high frequency calculated for ϕ_{10}' is due to the strong interaction with the B_{2g} pyrrole translation mode ν_{35} (109 cm^{-1}), as mentioned above. Both modes have a natural frequency of ~200 cm^{-1} (ν_{35} = 197 cm^{-1} for NiP) and undergo a near-resonant interaction. The interaction is reflected in a ~3-cm^{-1} d_{20} downshift of ν_{35} (Table VII).

Polarized bands are found with Soret excitation which are assignable to all the A_{1g} phenyl modes (ϕ_4–ϕ_{10}) except for the C–H stretches. In every case except ϕ_{10} the intensity is attributable to mixing with nearby A_{1g} porphyrin skeletal mode; the ϕ_{10} (203 cm^{-1}) intensity is no doubt due to the major involvement of C_m–Ph bond stretching, as discussed above. An example of phenyl–porphyrin mode mixing is illustrated in Figure 15 showing the eigenvectors of the prominent phenyl mode ϕ_4 (1599 cm^{-1}) and the very strong nearby ν_2 skeletal mode (1572 cm^{-1}). The eigenvectors show nearly the same atomic motions but with opposite phases. The mixing results in a 4 cm^{-1} *up*shift of ν_2 upon phenyl perdeuteration (d_{20}) as the interaction is relieved by the large downshift of ϕ_4. Other interactions involve ϕ_5 with ν_{11}, ϕ_6 with ν_1, and ϕ_7 and ϕ_8 with ν_6. The near-resonant interaction of ϕ_9 and ν_7, resulting in large frequency shifts and intensity transfer

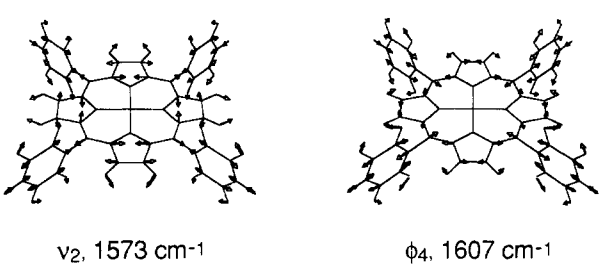

Figure 15. Eigenvectors of ν_2 and the adjacent phenyl mode ϕ_4, showing coordinate mixing.

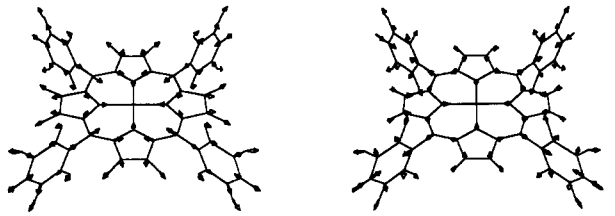

Figure 16. Eigenvectors of ν_7 and ϕ_9 showing nearly equal contribution from pyrrole and phenyl deformation coordinates.

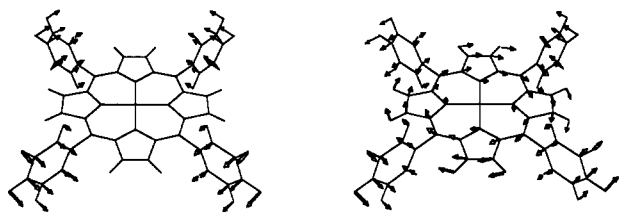

Figure 17. Eigenvectors of the calculated π_6 (A_{1g}) and π_6' (B_{2g}) phenyl bending mdoes.

to ϕ_9, was discussed above. The eigenvectors of these modes are shown in Figure 16.

The B_{1g} phenyl modes, ϕ_i', are not seen with the exception of ϕ_7' which is identified with a very weak band at 1052 cm^{-1} (Figure 10) on the basis of isotope shifts (Table VIII). Most of the ϕ_i' bands would be obscured by other bands at their expected positions.

Four of the out-of-(phenyl)plane modes can be identified as weak low-frequency bands in the Q-band-excited spectra (vibronic activation) via their isotope shifts. Two of these are symmetric CH wags (all CH bonds bend toward the same side of the phenyl ring), π_3 and π_3' at 701 and 684 cm^{-1} (Figure 11). The other two are ring deformations, π_4 and π_5 at 498 and 390 cm^{-1}. Because the depolarization measurements in the KCl pellets are not quantitative it is difficult to distinguish between B_{2g} (dp) and A_{2g} (ap) assignments.

We call attention to the very low frequency modes π_6, π_6', and π_6'' calculated at 45–83 cm^{-1}. These modes involve a bending motion of the entire phenyl ring relative to the C_m–Ph bond, as illustrated in Figure 17. Jortner and co-workers[37] observed very strong emission bands in this frequency region for free base TPP and its Zn and Mg complexes in a free-expansion jet. Although they tentatively attributed these bands to phenyl torsional modes, the torsions are expected[38] at somewhat higher frequencies, and moreover, are expected to be weak since they transform as the porphyrin out-of-plane modes. Assignment to the π_6 phenyl bands is suggested.

Inasmuch as the phenyl rings of TPP are oriented perpendicular to the porphyrin plane the π systems are not in conjugation. Consistent with this inference, NMR data show little electronic delocalization onto the phenyl groups.[39] It has been suggested[8] that the substantial RR enhancements seen for the phenyl modes reflect delocalization in the excited state perhaps reflecting phenyl rotation toward the porphyrin plane. In view of the interactions of the prominent phenyl modes with nerby porphyrin skeletal modes, however, it seems likely that their intensity is borrowed via vibrational coupling. There is no qualitative evidence for phenyl delocalization. Surprisingly, there is qualitative evidence for electronic involvement of the ethyl groups in the excited states

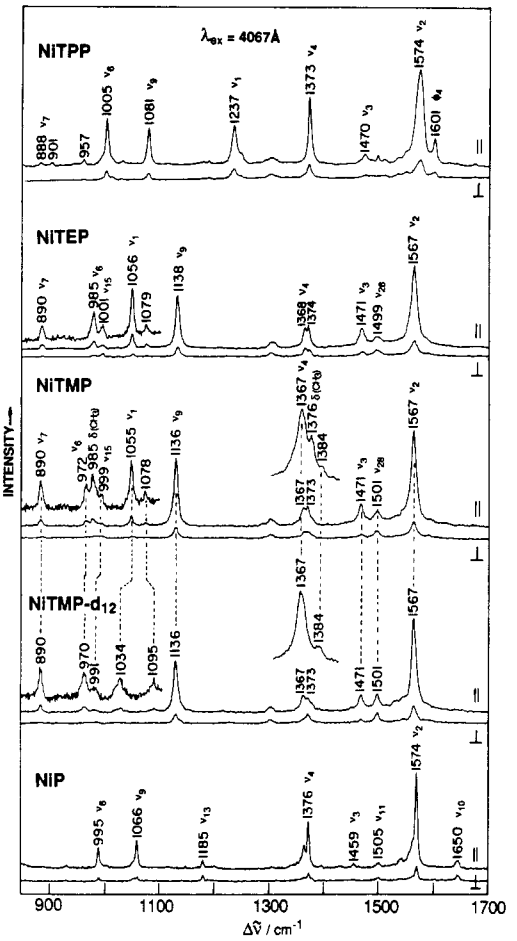

Figure 18. RR spectra with 4067-Å excitation for Ni^{2+} complexes of TPP, TEP, TMP (and its methyl-d_{12} isotopomer), and P, in CS_2 solution. Shown as insets are expanded views of the 850–1100-cm^{-1} regions and of the NiTMP 1370-cm^{-1} region; the latter was obtained with 4579-Å excitation and shows the methyl deformation mode at 1376 cm^{-1}, which disappears in the d_{12} isotopomer. Conditions: 150 mW, 4 cm^{-1} slit widths.

of NiOEP, as discussed in the succeeding article.[14a]

6. Meso Substitution Systematics: NiTMP and NiTEP. Having analyzed the effect of phenyl substitution at the porphine meso carbon atoms, we thought it worthwhile to take a brief look at the effects of methyl or ethyl substitution at the meso positions. Figure 18 compares RR spectra with Soret excitation for NiTMP (TMP = *meso*-tetramethylporphyrin) and NiTEP (TEP = *meso*-tetraethylporphyrin) with those of NiP and NiTPP. The effect of deuterating the NiTMP methyl groups is also shown. Andersson et al.[40] have examined the NiTMP spectrum and assigned the strong band at ~1140 cm^{-1} to the porphyrin–methyl stretch (ν_1). This assignment is ruled out, however, by the absence of any methyl deuteration shift. Instead the weak band at 1055 cm^{-1} is assigned to the porphyrin methyl stretch, ν_1, based on its 21 cm^{-1} d_{12} shift. Another weak band, at 985 cm^{-1}, disappears upon methyl deuteration (see inset) and is assigned to the rocking mode of the methyl groups which is normally seen in this frequency region.[24] Finally an extra band on the side of ν_4, at 1376 cm^{-1}, also disappears upon methyl deuteration and is assigned to the $\delta(CH_3)$ band (umbrella mode). These assignments complete the list of expected methyl contributions. An additional weak band is seen at 1078 cm^{-1}, which appears to shift up by 17 cm^{-1} upon methyl deuteration; this is attributed to a combination mode which interacts with the methyl modes. The same band pattern is seen for NiTEP, and the same assignments no doubt apply, except that the methylene CH deformations take the place of the methyl CH deformations.

(37) (a) Even, U.; Magen, J.; Jortner, J.; Friedman, J.; Levanon, H. *J. Chem. Phys.* **1982**, *77*, 4374. (b) Even, U.; Magen, J.; Jortner, J.; Levanon, H. *J. Chem. Phys.* **1987**, *76*, 5684.

(38) (a) Im, H.-S.; Bernstein, E. R. *J. Chem. Phys.* **1988**, *88*, 7337. (b) Kirin, D. *J. Phys. Chem.* **1988**, *92*, 3691.

(39) (a) La Mar, G. N.; Eaton, G. R.; Holm, R. H.; Walker, F. A. *J. Am. Chem. Soc.* **1973**, *95*, 63. (b) Walker, F. A.; Balke, V. L.; McDermott, G. A. *J. Am. Chem. Soc.* **1982**, *104*, 1509.

(40) Andersson, L. A.; Loehr, T. M.; Sotirius, C.; Wu, W.; Chang, C. K. *J. Am. Chem. Soc.* **1986**, *108*, 2908.

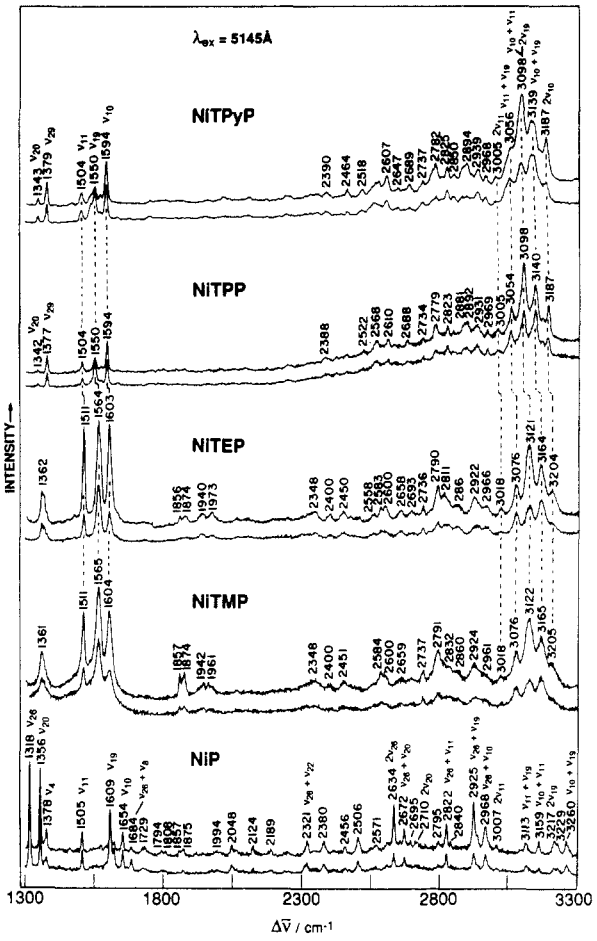

Figure 19. RR spectra with 5145-Å excitation for Ni^{2+} complexes of the indicated porphyrin in KCl pellets, showing extensive activation of overtone and combination bands.

The only candidate for the strong 1136-cm^{-1} band, seen in both NiTMP and NiTEP, is the $\delta(C_\beta H)$ band ν_9, shifted up 70 cm^{-1} from its frequency in NiP. It is also relevant that ν_6 appears to shift down ($\sim$25 cm^{-1}) slightly from NiP and loses much of its intensity, while ν_9 becomes stronger. The total ν_9 plus ν_6 intensity appears to be roughly constant. This observation suggests that ν_6 and ν_9 interact strongly in NiTMP and NiTEP, but not in NiP, the interaction evidently being turned on by the involvement of the methyl or ethyl substituents. The kinematics of this effect remain to be elucidated. However, it could be related to the decreased effective symmetry of NiTMP and NiTEP due to the alkyl substitution, discussed below.

Other spectral alterations include an intensification of ν_3 (1471 cm^{-1}) in NiTMP and NiTEP relative to both NiP and NiTPP, suggesting some unmixing of the $\nu(C_\beta C_\beta)$ and $\nu(C_\alpha C_m)$ coordinates which account (see above) for the ν_3 weakness.

Another point of interest concerns the polarization of the ν_{19} and ν_{10} bands, which can be seen in the 514.5-nm-excited spectra (Figure 19). These are ap and dp for NiP and NiTPP, as expected, the symmetries being A_{2g} and B_{1g}. For NiTMP and NiTEP, however, they become dp and p, respectively. Their frequencies and relative intensities leave no room for any other assignments, and the altered polarizations must be attributed to a lowering of the effective symmetry from D_{4h}. The polarization pattern requires loss of two of the in-plane C_2 axes, producing the D_2 point group, in which the mode correlations are $A_{2g}(ap) \rightarrow B_1(dp)$ and $B_{1g}(dp) \rightarrow A(p)$. Since the modes in question involve $C_\alpha C_m$ stretching primarily, it can be inferred that the symmetry lowering is due to the altered meso substituents. In fact the substituents do lower the symmetry since neither the ethyl nor the methyl group has a C_2 axis; the porphyrin C_2'' axes which pass through the methine bridges are therefore lost. For TPP the C_2'' axes are maintained because the phenyl groups do share these axes.

Figure 19 shows dramatically strong overtone and combination band intensities in the 2500–3500-cm^{-1} region for all of the complexes under study with excitation in the Q_1 band. This effect has been observed previously by Aramaki et al.[41] for CuTPP, by Gladkov et al. for CuP,[42] and by Friedman and Hochstrasser et al. for cytochrome c,[43a,b] and is attributable to the third term in the Taylor series expansion of the Raman tensor, called the C term by Ziegler and Hudson.[44] This term involves the square of the transition moment derivative with respect to the normal coordinate. It requires vibronic integrals involving one quantum changes for both the up and the down transition, i.e., a two-quantum Raman transition overall. Ordinarily this term is much less important than the A or B terms, but both of the latter terms (which involve the square of the transition moment and the product of the transition moment and its derivative, respectively) are zero when the transition moment is zero, and only the C term survives. Thus the C term becomes important for resonance with strongly forbidden electronic transitions, as has been demonstrated[44] for the $^1B_{1u}$ state of benzene. The Q transition of metalloporphyrins is quasi-forbidden, due to the near cancellation of the $a_{2u} \rightarrow e_g$ and $a_{1u} \rightarrow e_g$ transition dipoles. The Q-band-excited overtone and combination band intensities become relatively prominent as the Q_0 intensity decreases; moreover, maximum enhancement for this mechanism is expected, and observed,[41] at the Q_1 wavelength.

The Q_0 intensity is relatively small for NiP and is even smaller for the meso-substituted analogues (the NiTMP and NiTEP spectra are similar to that of NiTPP, shown in Figure 4). Several combination bands are prominent for NiP (Figure 19) expecially those involving the very strong ν_{26} fundamental, which builds a sequence with ν_{22}, ν_{20}, ν_{11}, ν_{19}, and ν_{10}. Since ν_{26} involves C_mH bending, primarily, it is missing in the meso-substituted analogues, for which ν_{11}, ν_{19}, and ν_{10} are the strongest fundamentals with Q_1 band excitation. As seen in Figure 19 these produce combination bands which are nearly as strong as the fundamentals, consistent with the low Q_0 absorption strengths.

Conclusions

The in-plane Raman frequencies of NiP and NiTPP (and the IR frequencies for NiP), as well as extensive isotopic frequency shifts, can be accounted for with a physically plausible force field. Only minor force constant changes are needed to accommodate the phenyl substitution in TPP. The principal force constants are in good accord with bond length relationships selected on the basis of recent scaled ab initio calculations. Essentially all of the in-plane porphyrin modes are accounted for. These modes are classifiable on the basis of local coordinates which take into account the mutual phasing of the pyrrole bond stretches and of the bridge bond stretches. The good agreement among most of the frequencies assigned to a given local coordinate indicate that, with a few exceptions, longer range phasings have little influence.

Substitution of phenyl groups at the C_m atoms has a relatively small effect on the skeletal mode frequencies, but the asymmetric $C_\alpha C_m$ stretches, $\nu_{10}(B_{1g})$ and $\nu_{19}(A_{2g})$ are lowered significantly (60 cm^{-1}), an effect attributed partly to removal of the interaction with C_mH bending and partly to an electronic effect of the phenyl groups resulting in an increased $C_\alpha C_m$,$C_\alpha C_m$ stretch–stretch interaction force constant. Another effect is kinematic coupling between deformation modes of the pyrrole rings and of the phenyl rings, both near 750 cm^{-1}, resulting in pairs of displaced modes near 880 and 640 cm^{-1}. Most of the intensity accumulates in the lower frequency mode of this pair, which is nevertheless allocated

(41) Aramaki, S.; Hamaguchi, H.; Tasumi, M. *Chem. Phys. Lett.* **1983**, *96*, 555.
(42) Gladkov, L. L.; Gradyushko, A. T.; Ksenofontova, N. M.; Solovyov, K. N.; Starukhin, A. S.; Shulga, A. M. *J. Appl. Spectrosc.* **1978**, *28*, 462 (Engl. Transl.).
(43) (a) Friedman, J. M.; Hochstrasser, R. M. *Chem. Phys.* **1973**, *1*, 457–467. (b) Friedman, J. M.; Hochstrasser, R. M. *J. Am. Chem. Soc.* **1976**, *98*, 4043.
(44) Ziegler, L. D.; Hudson, B. *J. Chem. Phys.* **1981**, *74*, 982.
(45) (a) Meyer, E. F., Jr. *Acta Crystallogr.* **1972**, *B28*, 2162. (b) Cullen, D. L.; Meyer, E. F., Jr. *J. Am. Chem. Soc.* **1974**, *96*, 2095. (c) Brennan, T. D.; Scheidt, W. R.; Shelnutt, J. A. *J. Am. Chem. Soc.* **1988**, *110*, 3919.

to a phenyl mode because of its larger d_{20} shift. Other phenyl modes are also seen and their intensity is likewise attributable to coupling with nearby porphyrin modes. There is no qualitative evidence for significant electronic coupling between the porphyrin and phenyl π systems, although a quantitative intensity analysis is needed to evaluate the extent of coupling.

The surprisingly large intensity of the $C_\beta H$ bending mode of NiP implies a significant change in the $C_\beta H$ bond angle in the excited state, while the intensity of the B_{1g} C_mH bending mode implies a significant change in the C_mH bond angle via an excited-state Jahn-Teller effect. Substitution of methyl or ethyl groups at the meso-carbon atoms produces somewhat different kinematic effects than phenyl substitution; modes of the alkyl substituents can be seen. The alkyl groups lower the effective molecular symmetry, as reflected in the $C_\alpha C_m$ stretching band polarization, probably due to orientation effects. All the Ni porphyrins show strong overtone and combination band enhancements in resonance with the Q_1 transition, reflecting the small Q_0 transition moment and the resulting importance of C term RR scattering.

Acknowledgment. This work was supported by NIH grants GM 33576 (T.G.S.) and DK 35153 (J.R.K.).

Registry No. NiP, 15200-33-6; NiTPP, 14172-92-0; D, 7782-39-0; N, 14390-96-6; ^{13}C, 14762-74-4.

Supplementary Material Available: Atom numbering schemes for NiP (35 atoms) and NiTPP (77 atoms) with D_{4h} symmetries and characteristics of the porphyrin in-plane valence force field (Figures 1-3), Cartesian coordinates for NiP and NiTPP, definition of internal coordinates for NiP and NiTPP, and unnormalized U matrices for A_{1g}, A_{2g}, B_{1g}, B_{2g}, and E_u symmetry blocks of NiP and NiTPP (Tables 1-6) (21 pages). Ordering information is given on any current masthead page.

Consistent Porphyrin Force Field. 2. Nickel Octaethylporphyrin Skeletal and Substituent Mode Assignments from ^{15}N, Meso-d_4, and Methylene-d_{16} Raman and Infrared Isotope Shifts

Xiao-Yuan Li,[†] Roman S. Czernuszewicz,[†] James R. Kincaid,[‡] Paul Stein,[§] and Thomas G. Spiro*,[†]

Department of Chemistry, Princeton University, Princeton, New Jersey 08544, Department of Chemistry, Marquette University, Milwaukee, Wisconsin 53233, and Department of Chemistry, Duquesne University, Pittsburgh, Pennsylvania 15282 *(Received: December 20, 1988)*

Resonance Raman spectra with variable-wavelength excitation are reported for nickel octaethylporphyrin and its isotopomers containing ^{15}N, and ^2H at the methine (meso-d_4) and methylene (methylene-d_{16}) carbon atoms. The ^{15}N, meso-d_4 double isotopomer is also examined. The infrared spectrum of the methylene-d_{16} isotopomer is reported, and the frequencies are combined with recently published infrared results for the other isotopomers. Essentially all of the porphyrin skeletal modes have been assigned and have been allocated to local coordinates which recognize the pyrrole rings as cooperative vibrational units. The assignments are supported by a normal-coordinate analysis with a valence force field involving standard ethyl force constants and porphyrin in-plane force constants which are transferred nearly intact from Ni porphine and Ni tetraphenylporphyrin. Many vibrational modes of the NiOEP ethyl substituents have also been located in the spectra and assigned. Bands assignable to ethyl C-C stretching and C-H bending modes are surprisingly strong in the resonance Raman spectra and suggest appreciable involvement of the ethyl groups in the porphyrin π-π^* excited states. The conformations of the ethyl substituents have a marked influence on the low-frequency vibrational spectra.

Introduction

Nickel octaethylporphyrin (NiOEP) has played a key role in the characterization of heme proteins by resonance Raman (RR) spectroscopy.[1,2] Like all physiological porphyrins, OEP has carbon substituents at the eight pyrrole positions, and it retains the 4-fold symmetry of the porphyrin skeleton (neglecting questions of ethyl orientation), so that symmetry considerations can be brought fully to bear on the vibrational analysis. Kitagawa and co-workers[3] carried out an important base-line study of NiOEP using ^{15}N and meso-d_4 isotope shift data to assign most of the in-plane skeletal modes of the porphyrin ring in a consistent fashion, and they carried out a normal-coordinate calculation with a modified Urey-Bradley force field. They assumed that the ethyl substituents were isolated from the porphyrin electronic system and did not contribute directly to the RR spectra; the substituents were in fact treated as point masses. While this was a reasonable starting approximation, there have since been indications that it breaks down, especially in the 900-1300-cm^{-1} and in the low-frequency region of the spectrum, where porphyrins with different pyrrole substituents show appreciable spectral differences.[4]

We have therefore undertaken to examine the question of ethyl-substituent involvement in the NiOEP vibrational spectra via replacement of the methylene hydrogen atoms with deuterium. The results are striking; some of the strongest bands in the $\sim$ 1000-cm^{-1} region are attributable to modes which are predominantly ethyl in character, as revealed by their methylene-d_{16} shifts. These enhancements imply involvement of the ethyl groups in the porphyrin π-π^* excited states. The low-frequency region of the

* Author to whom correspondence should be addressed.
[†] Princeton University.
[‡] Marquette University.
[§] Duquesne University.

(1) Spiro, T. G.; Li, X.-Y. In *Biological Applications of Raman Spectroscopy*; Spiro, T. G., Ed.; Wiley-Interscience: New York, 1988; Vol. III, Chapter 1.
(2) Kitagawa, T.; Ozaki, Y. *Struct. Bonding (Berlin)* **1987**, *64*, 71-114.
(3) (a) Kitagawa, T.; Abe, M.; Ogoshi, H. *J. Chem. Phys.* **1978**, *69*, 4516-4525. (b) Abe, M.; Kitagawa, T.; Kyogoku, Y. *J. Chem. Phys.* **1978**, *69*, 4526. (c) The calculations in ref 3a and 3b have been revised slightly in a recent review by: Abe, M. In *Spectroscopy of Biological Systems*; Clark, R. J. H., Hester, R. E., Eds.; Wiley: New York, 1986; Vol. 13, Chapter 7.
(4) (a) Choi, S.; Spiro, T. G.; Langry, K. C.; Smith, K. M. *J. Am. Chem. Soc.* **1982**, *104*, 4337. (b) Choi, S.; Spiro, T. G.; Langry, K. C.; Smith, K. M.; Budd, L. D.; La Mar, G. N. *J. Am. Chem. Soc.* **1982**, *104*, 4345.

0022-3654/90/2094-0047$02.50/0